The Luminescence of Divalent Europium in $Cs_2Ca^{2+}P_2O_7$ and $Cs_2Sr^{2+}P_2O_7$

by

Stephen B. Chaney

(Under the direction of Uwe Happek)

Abstract

The excitation and emission spectra of the octahedrally coordinated Eu^{2+} ion in $Cs_2M^{2+}P_2O_7$, where M = Ca and Sr, is reported and discussed. The remarkable features of the Eu^{2+} luminescence in these double phosphate materials include (a) the very large Stokes shift of emission (1 eV), (b) the high luminescence quenching temperature and (c) the very low energy of the emitted photons, which is unusual for the luminescence of the Eu^{2+} ion in phosphate based materials. The broad emission bands of Eu^{2+} in $Cs_2CaP_2O_7$ and $Cs_2SrP_2O_7$ peak at 607 nm and 563 nm, respectively. The Stokes shift, crystal field splitting, the centroid shift and the red shift of the Eu^{2+} $4f^6 5d^1$ electronic configuration have been estimated from the relevant optical data. The radiative lifetime of the Eu^{2+} emission in $Cs_2M^{2+}P_2O_7$ is $\approx$ 1.2 μs. The nature of the Eu^{2+} emission in $Cs_2M^{2+}P_2O_7$ is discussed and arguments are presented to associate the luminescence with the normal $4f^6 5d^1$ $4f^7[^8S_{7/2}]$ emission transition. A discussion of the characteristic properties of the "anomalous" emission of the Eu^{2+} ion in solids is also presented and compared with the properties of the Eu^{2+} luminescence in $Cs_2M^{2+}P_2O_7$.

Index words: Divalent europium, scintillator, materials science, luminescence, condensed matter physics, octahedral symmetry, $Cs_2CaP_2O_7$:Eu^{2+}, $Cs_2SrP_2O_7$:Eu^{2+}, Dissertations (academic)

The Luminescence of Divalent Europium in $Cs_2Ca^{2+}P_2O_7$ and $Cs_2Sr^{2+}P_2O_7$

by

Stephen B. Chaney

B.S., Augusta State University, 2003

A Dissertation Submitted to the Graduate Faculty
of The University of Georgia in Partial Fulfillment
of the
Requirements for the Degree

Doctor of Philosophy

Athens, Georgia

2009

The Luminescence of Divalent Europium in $Cs_2Ca^{2+}P_2O_7$ and $Cs_2Sr^{2+}P_2O_7$

by

Stephen B. Chaney

Approved:

Major Professor: Uwe Happek

Committee: Michael Geller
William Dennis

Electronic Version Approved:

Maureen Grasso
Dean of the Graduate School
The University of Georgia
May 2009

Dedication

This is dedicated to the ones that I love. To all those who have helped along the way. To my parents. Thank you for never giving up on me and for all of your help through the years. To my brother and sister. Thank you for being inspirations to me. Tyffani, your free spirit and endless cheerfulness are always encouraging and our conversations are always uplifting. Eric, what can I say? You have always been a great friend and confidant. You are my twin. What more needs to be said?

To my children Isabella, Sophia, Nathanael & Isaac. Your love and enthusiasm for life has sustained and grounded me throughout this entire experience. Especially you Isabella, you have borne the heaviest of all the burdens. What wonderful joys you all are.

And finally, to my loving wife. You are my compass and my guide. My love for you over these years has continually grown and intensified. Thank you for being you. Your love is always encouraging. Your fire is always refining my character and your support will always be cherished.

Acknowledgments

This work would not be possible without the aid of many contributors. It was supported in part by General Electric under a cooperative funding initiative.

My advisor, Uwe Happek, whose direction and supervision have led me to a greater understanding of experimental condensed matter physics and general applied physics. I would also like to thank General Electric for providing numerous samples for testing and for the discussions with colleagues at GE's Global Research Center. Thank you to all of the members of the Happek group who have discussed problems and solutions and for their friendship over the course of my graduate career. Especially, Murat Aycibin who made significant contributions to this work, Steve Compton for many discussions and for proofreading this manuscript, and the other members of the Happek group Mark Hannah and Long Pham.

Table of Contents

List of Figures

List of Tables

Chapter 1

Introduction

1.1 Background

Phosphors play an important role in the world around us. They are present in a wide range of devices including LED's, medical imaging devices, cell phone displays, CRT televisions, flat panel displays and communications systems. Phosphors usually are transition metal or rare-earth metal containing compounds and research into the understanding of these materials is a complex area that has many aspects. Europium, a rare-earth metal, is a common dopant in phosphor materials. It is the purpose of this dissertation to expand the understanding of the optical properties of the divalent europium (Eu^{2+}) ion when it occupies a six-coordinated octahedral site in solids. Specifically, the investigations on the luminescence of the Eu^{2+} ion in the diphosphates, $Cs_2CaP_2O_7$ and $Cs_2SrP_2O_7$ is presented.

Europium was discovered in the late 1800's and finally isolated in 1901. It has most notably been used in the form of Eu_2O_3 as the phosphor that provides the brilliant red color in CRT televisions and fluorescent lamps. It has two stable oxidation states: Eu^{2+} and Eu^{3+}. Europium(III) is typically pumped via a charge transfer transition in the near ultra-violet region of the electromagnetic spectrum and the emission is characterized by sharp lines in the red to near infrared. Eu^{2+} is characterized by broad dipole-allowed absorption and emission bands. The current literature reports absorption in the UV to near UV and emission in the wavelength range of 390–490 nm [1]. However, a few Eu^{2+} compounds have demonstrated emission into the red.

The dependence of the Eu^{2+} emissions upon the host material can be interpreted by examining the europium ion. In the divalent state, europium has seven f electrons which

form a stable half-filled $4f$ valence shell. These seven electrons are tightly bound to the positively charged nucleus and do not interact strongly with the environment of the host system. Upon excitation, a $4f^7$ electron is excited into the $5d$ state. The wavefunctions of this state extend much farther from the nucleus and thus interacts strongly with the neighboring host ions.

1.2 Current Research

The optical characteristics of divalent europium as an impurity ion in inorganic compounds has been investigated extensively [2–5]. The octahedrally coordinated Eu^{2+} ion is of particular interest and a wide range of compounds containing this coordination are found in the literature. Specifically, the excitation and emission data of Eu^{2+} in the octahedral environments of alkali halides, alkaline earth sulfides, selenides, flouride perovskites such as $M^{+}CaF_3$ (M = Cs, Rb, K), $LiCaAlF_6$, alkaline earth oxides $M^{2+}O$ (M = Ca, Sr)[6], and alkaline earth pyrophosphates [7]. A list of over 300 Eu^{2+} ion containing compounds and there corresponding spectroscopic properties has been compiled and analyzed by Dorenbos [1].

The energy level scheme of the Eu^{2+} ion in an octahedral site is given in Figure 1.1. The $^8S_{7/2}$ ground state of the Eu^{2+} ion is spherically symmetric and upon excitation the octahedral field splits the $4f^6 5d^1$ state into two states. The lower state is triply degenerate containing the d_{xy}, d_{zx}, and d_{yz} orbitals and is denoted t_{2g}. The higher energy state, labeled e_g, is doubly degenerate consists of the $d_{x^2-y^2}$ and d_{z^2} orbitals. The separation between the centroids of the e_g and t_{2g} levels is defined as the crystal field splitting ($10Dq$). In the octahedral field, the absorption or excitation spectra of Eu^{2+} ions are characterized by two well separated broad bands. The low and high energy bands are attributed to the $4f^7[^8S_{7/2}] \rightarrow 4f^6 5d^1[t_{2g}]$ and $4f^7[^8S_{7/2}] \rightarrow 4f^6 5d^1[e_g]$ optical transitions respectively. It is well documented that the t_{2g} band may exhibit a so called "staircase" spectrum [8, 9]. This staircase spectrum is due to the transitions from the $^8S_{7/2}$ ground state to the ^7F_J (J=0–6) multiplets of the excited $4f^6[^7F_J]5d^1$ electronic configuration.

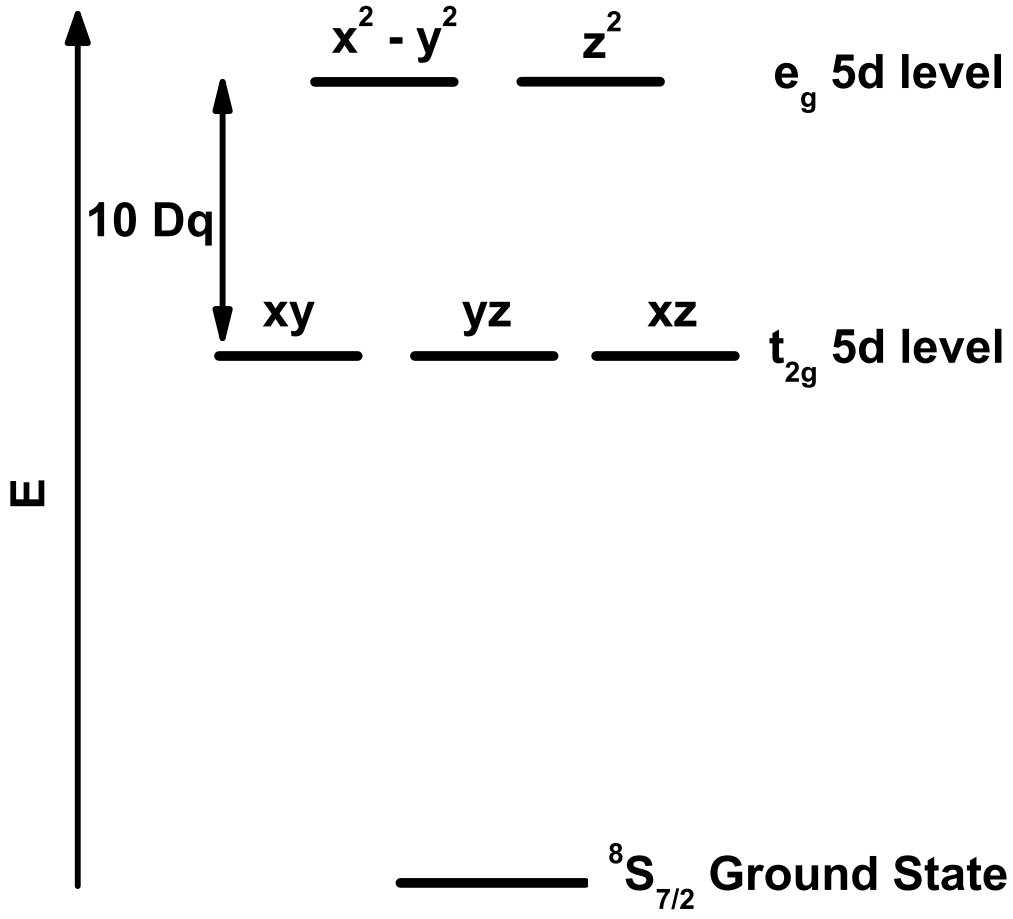

Figure 1.1: Splitting of divalent europium in an octahedral ligand field

When the site symmetry of the Eu^{2+} ion is lower than that of an octahedron, the total crystal field splitting and the centroid shift of the $4f^6 5d^1$ electronic configuration are difficult to determine. This is due to the complicated nature of the Eu^{2+} $4f^6 5d^1$ energy level scheme [9]. Therefore the evaluation of these parameters are limited to the discussion of compounds containing either an octahedral cubal, or cubo-octahedral site symmetry [10, 11].

This present work focuses on the optical properties of the Eu^{2+} doped pyrophosphate compounds $Cs_2CaP_2O_7$ and $Cs_2SrP_2O_7$. In chapter 2, a brief theoretical development of the octahedrally coordinated divalent europium ion and general spectroscopic techniques that were used to characterize the materials will be reviewed. This will include the crystal structure of the materials studied, europium doping, the ligand field theory of octahedrally coordinated systems, and the use of absorption and emission spectra in the determination of material properties. The third chapter will describe all of the experimental details including the synthesis of the materials, presentation of apparatus schematics, and experimental conditions. Chapter 4 is the presentation of results. Chapter 5 is a discussion of the many details surrounding the behavior of the divalent europium emission in our pyrophosphates and materials studied by others. Lastly, the sixth chapter contains a general summary.

1.3 References

[1] P. Dorenbos, J. Lumin., **104**, 239, (2003).

[2] P. M. Jaffe, J. Electrochem. Soc.:Solid State Sci., **117**, 918, (1970).

[3] C. K. Duan, M. F. Reid, J. Sol. State Chem., **171**, 299, (2003).

[4] C. K. Duan, M. F. Reid, Phys. Rev. B., **66**, 155108, (2002).

[5] J. Hernandez A., W. K. Cory, and J. Rubio O., J. Chem. Phys., **72**, 198, (1980).

[6] J. Overmeyer and R. J. Gambino, Phys Lett., **9**, 108, (1964).

[7] W. L. Wanmaker and J. W. ter Vrugt, Phil. Res. Rep., **22**, 355, (1967).

[8] M. J. Freiser, S. Methfesskl, and F. Holtzberg, J. App. Phys., **39**, 900, (1968).

[9] F. M. Ryan, W. Lehmann, D. W. Feldman, and J. Murphy, J. Electrochem. Soc., **121**, 1475, (1974).

[10] D. McClure and Z. Kiss, J. Chem. Phys., **39**, 3251, (1963).

[11] P. Dorenbos, J. Phys.: Condensed Matter, **15**, 4797, (2003).

[12] G. Blasse, J. Chem. Phys., **51**, 3529, (1969).

Chapter 2

Review of Divalent Europium and Spectroscopic Techniques

2.1 Divalent Europium Doping

The atomic configuration of the lanthanide rare-earth metals are characterized by inner electrons that occupy the $4f$ shell. These f shell electrons are shielded by valence electrons in the $6s$ level and sometimes a $5d$ electron where the typical configuration is $[\mathrm{Xe}]4f^n5d^{(1\,or\,0)}6s^2$.

Europium has an electronic structure of $[\mathrm{Xe}]4f^76s^2$ and with the ground state $^1S_0$. In the divalent state it is coordinated as $[\mathrm{Xe}]4f^7$ having a ground state of $^8\mathrm{S}_{7/2}$ and the first excited state is the $[\mathrm{Xe}]4f^65d^1$. The f electrons of europium are well localized and have strong enough interactions to produce local magnetic moments.

Recently, it has been proposed by Dorenbos [13–15] that by determining the first $5d$ level energy of one specific Lanthanide ion within a given crystalline environment, one can determine all other $5d$ level energies for all other lanthanides in the same compound. Of specific interest are the relationships between Ce^{3+} and Eu^{2+}. Dorenbos contends that the Stokes shift of emission, the centroid shift of the $5d$ configuration and the total crystal field splitting ($10Dq$) are all linearly related to one another [16].

In an idealized lanthanide crystal system (Band diagram in Figure 2.1) there are three assumptions to be made: (1) the interaction between the excited $5d$ electron and the remaining core of the lanthanide ion is identical for each lanthanide; (2) the interaction between the $5d$ electron and the crystalline environment is identical for each lanthanide; and (3) the lattice relaxation around the lanthanide ion is always the same despite the lanthanide contraction of 20 pm from the beginning to the end of the lanthanide series. The energy difference between the first $5d$ level of the lanthanide and the conduction band of

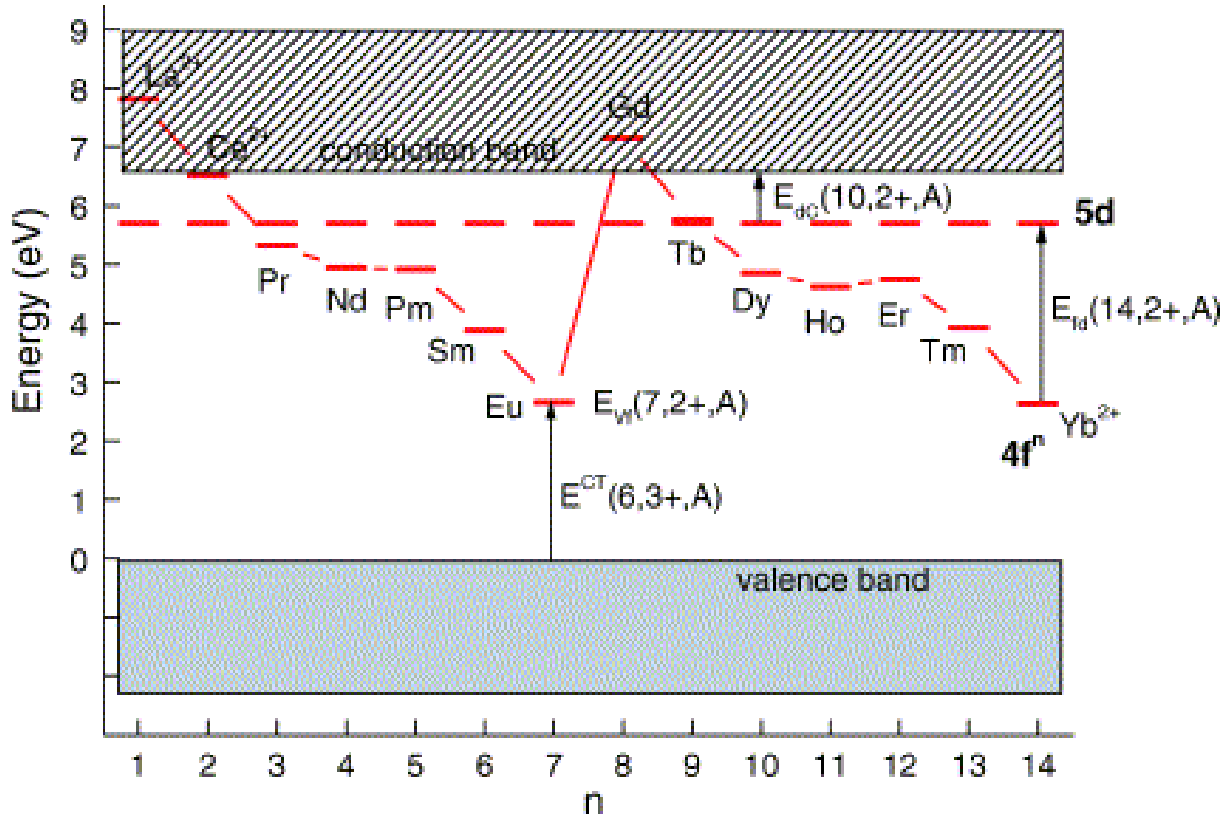

Figure 2.1: This is an idealized systematic of the energy-level positions of divalent lanthanides in a wide band gap ionic crystal. Where n represents the number of electrons in the f level, E^{CT} is the charge transfer energy gap.

the crystal host (denoted as E_{dC}) will be constant for all lanthanides [17]. One would have the natural inclination that the true nature of these lanthanides should vary from atom to atom. The results of hundreds of experiments were compiled and evaluated to show that indeed this variation is seen. There are some general trends that emerge from the data.

The general relationship

$$E_{fd}(n, 2+, A) = E_{Afree}(n, 2+) - D(2+, A) \tag{2.1}$$

describes the energy for the first $f \rightarrow d$ transition for all other lanthanides if the $E_{fd}(n, 2+, A)$ is known for any other lanthanide in compound A. It is simply the free ion energy ($E_{Afree}(n, 2+)$) minus the redshift ($D(2+, A)$). So if either the redshift or fd energy were to be measured, then a schematic for all other lanthanides is predictable. There are however a number of problems that can arise due to this idealization, including charge transfer transitions for the trivalent lanthanides, anomalous emission from the divalent lanthanides, and the overlap of the f electrons with the surrounding ligands.

2.2 Quantum Mechanics of Eu^{2+} in an Octahedral Ligand Field

The established crystal structures of the $Cs_2M^{2+}P_2O_7$ samples contain calcium and strontium sites that are six coordinated with oxygen that exhibits an octahedral symmetry. The methods of ligand field theory can describe the interaction of the Eu^{2+} ions with the nearest neighbor oxygen ions. Various texts and sources have been used in the development of the following discussion [18–24].

2.2.1 The Electronic Configuration of a $5d^1$ Electron in an Octahedral Ligand Field

The question now pertaining to this work is: how does divalent europium respond to an octahedral ligand field? To begin the task of unraveling the ligand field Hamiltonian for Eu^{2+} we first note that a $4f^7$ system has 3432 independent $|\alpha, S, L, J, M\rangle$, states [25]. Thankfully,

this is not what is observed experimentally as usually only the transitions from the $^8S_{7/2}$ ground state singlet to the ^5D excited state multiplet are of interest. These levels account for what is commonly referred to as the staircase spectrum and are seen as "steps" in the d excitation bands. Because the excited state of the Eu^{2+} ion contains a single d electron the system can be approximated by a hydrogen–like ion in an octahedral ligand field.

The ligand field Hamiltonian for a $5d$ electron is developed in the following manner. First we determine the central potential that the electron experiences as it sits (ideally) at a distance a from any one of its six nearest neighbor ions. Each ion has a charge of $-Ze$ and the electrostatic potential is

$$V(x,y,z) = V_x + V_y + V_z \tag{2.2}$$

where

$$V_x = -\frac{Ze}{4\pi\epsilon_0}\left[\frac{1}{(r^2+a^2-2ax)^{\frac{1}{2}}} + \frac{1}{(r^2+a^2+2ax)^{\frac{1}{2}}}\right] \tag{2.3}$$

with V_y and V_z having similar expressions with the independent variable exchanged and r is defined in the usual manner with $r^2 = x^2+y^2+z^2$. The octahedral crystal field can be expressed as $H_c^{O_h} = -eV$. If $r < a$ we can expand the Hamiltonian and in keeping the terms up to the sixth degree can obtain

$$\begin{aligned} V(x,y,z) &= \left[\frac{-1}{4\pi\epsilon_0}\frac{6Ze}{a} + \frac{35Ze}{4\pi\epsilon_0 4a^5}\left[(x^4+y^4+z^4) - \frac{3}{5}r^4\right]\right. \\ &+ \frac{21Ze}{4\pi\epsilon_0 2a^7}\left[(x^6+y^6+z^6)\right. \\ &+ \left.\left.\frac{15}{14}(x^2y^4+x^2z^4+y^2x^4+y^2z^4+z^2x^4+z^2y^4) - \frac{15}{14}r^6\right]\right] \end{aligned} \tag{2.4}$$

The crystal field Hamiltonian can then be expressed in terms of the spherical harmonics so that we can obtain [26]

$$\begin{aligned} \mathscr{H}_c^{O_h}(\mathbf{r}) &= \frac{Ze^2}{4\pi\epsilon_0}\left[\frac{6}{a} + \frac{7r^4}{2a^5}\left\{C_0^{(4)}(\theta,\phi) + \left(\frac{5}{14}\right)^{\frac{1}{2}}\left(C_4^{(4)}(\theta,\phi) + C_{-4}^{(4)}(\theta,\phi)\right)\right\}\right] \\ &+ \mathbf{r}^6\text{terms} + \ldots \end{aligned} \tag{2.5}$$

where $\mathbf{r}(r,\theta,\phi)$ is the position of the $5d$ electron and

$$C_t^{(k)}(\theta,\phi) = \left(\frac{4\pi}{2k+1}\right)^{1/2} Y_k^t(\theta,\phi). \tag{2.6}$$

We will ignore configuration mixing, although this does occur some in our system, and determine the effect of $\mathscr{H}_c^{O_h}$ on the $5d$ electron. When $l = 2$ as is the case for any d electron, we can ignore the terms in $\mathscr{H}_c$ that have power greater than four in r. We can also neglect the first term from Equation 2.5 because it is a constant term and will be added equally to each state and we are only interested in the energy differences. The matrix elements can then be calculated using the $|5dm_l\rangle$ states. Using Table 2.1 we can obtain the diagonal matrix element for the $|5d0\rangle$ state.

$$\langle 5d0|\mathscr{H}_c^{O_h}|5d0\rangle = \frac{1}{4\pi\epsilon_0}\frac{7Ze^2}{2a^5}\langle r^4\rangle_{5d}\frac{6}{21} = 6Dq \tag{2.7}$$

where

$$D = \frac{1}{4\pi\epsilon_0}\frac{35Ze^2}{4a^5} \quad \text{and} \quad q = \frac{2}{105}\langle r^4\rangle_{5d} \tag{2.8}$$

The Dq parameter is regarded as a single parameter that characterizes the strength of the octahedral crystal field. The matrix elements for all of the other non-vanishing terms can also be calculated and obtain the general crystal field matrix $\langle 5dm_l|\mathscr{H}_c^{O_h}|5dm_l'\rangle$. The matrix is

$$\begin{array}{c} \\ 5d2 \\ 5d1 \\ 5d0 \\ 5d-1 \\ 5d-2 \end{array} \begin{bmatrix} Dq & 0 & 0 & 0 & 5Dq \\ 0 & -4Dq & 0 & 0 & 0 \\ 0 & 0 & 6Dq & 0 & 0 \\ 0 & 0 & 0 & -4Dq & 0 \\ 5Dq & 0 & 0 & 0 & Dq \end{bmatrix} \tag{2.9}$$

and by diagonalizing it we obtain eigenstates ϕ_{t_2} (denoted as t_{2g} in this text) which are triply degenerate with the eigenvalues $-4Dq$ and the states ϕ_{e_2} (denoted as e_g in this text)which are doubly degenerate with eigenvalues of $6Dq$. The t_{2g} states extend in between the gaps of the ions whereas the e_g are localized on the ligand ions. The wavefunctions are listed below and the $10Dq$ splitting can be seen in Figure 2.2.

$$
\begin{aligned}
d_{z^2} &= \phi_{eu} = |5d0\rangle \\
d_{x^2-y^2} &= \phi_{ev} = \frac{1}{\sqrt{2}}\left(|5d2\rangle + |5d-2\rangle\right) \\
d_{yz} &= \phi_{t_2\xi} = \frac{i}{\sqrt{2}}\left(|5d1\rangle - |5d-1\rangle\right) \\
d_{xz} &= \phi_{t_2\eta} = -\frac{1}{\sqrt{2}}\left(|5d1\rangle - |5d-1\rangle\right) \\
d_{xy} &= \phi_{t_2\zeta} = -\frac{i}{\sqrt{2}}\left(|5d2\rangle - |5d-2\rangle\right)
\end{aligned}
\tag{2.10}
$$

In Figure 2.3, the graphical representation of the five atomic orbitals for a $5d$ electron is shown [30]. Each $5d_{xy}$, $5d_{xz}$, $5d_{yz}$, and $5d_{x^2-y^2}$ orbital has 12 lobes. There are two planar nodes normal to the axis of the orbital (so the $5d_{xy}$ orbital has yz and xz nodal planes, for instance). The $5d_{z^2}$ orbital is a little different and has two conical nodes. In addition, apart from the planar nodes, all five orbitals have two spherical nodes that partition off the small inner lobes. We notice that the d orbital is split into one higher energy doublet state and one lower energy triplet state. The crystal field can interact with this d electron strongly. If the symmetry of the octahedron is distorted, these two states will lose their degeneracy and become five distinguishable states.

2.3 Absorption, Emission, and Non-Radiative Decay

The following topics will rely heavily on the text by Henderson and Imbusch [24].

2.3.1 Absorption

Absorption is a measure of the interaction of electromagnetic radiation with matter. Put another way, it is the amount of energy that is lost when radiation passes through a material. This loss can be due to electronic or vibrational (phonons) (non-radiative) transitions. An experimental measurement of absorption is usually presented as a plot of absorbed intensity versus the incident photon energy ($E = h\nu$), frequency (ν), or wavelength (λ). While most

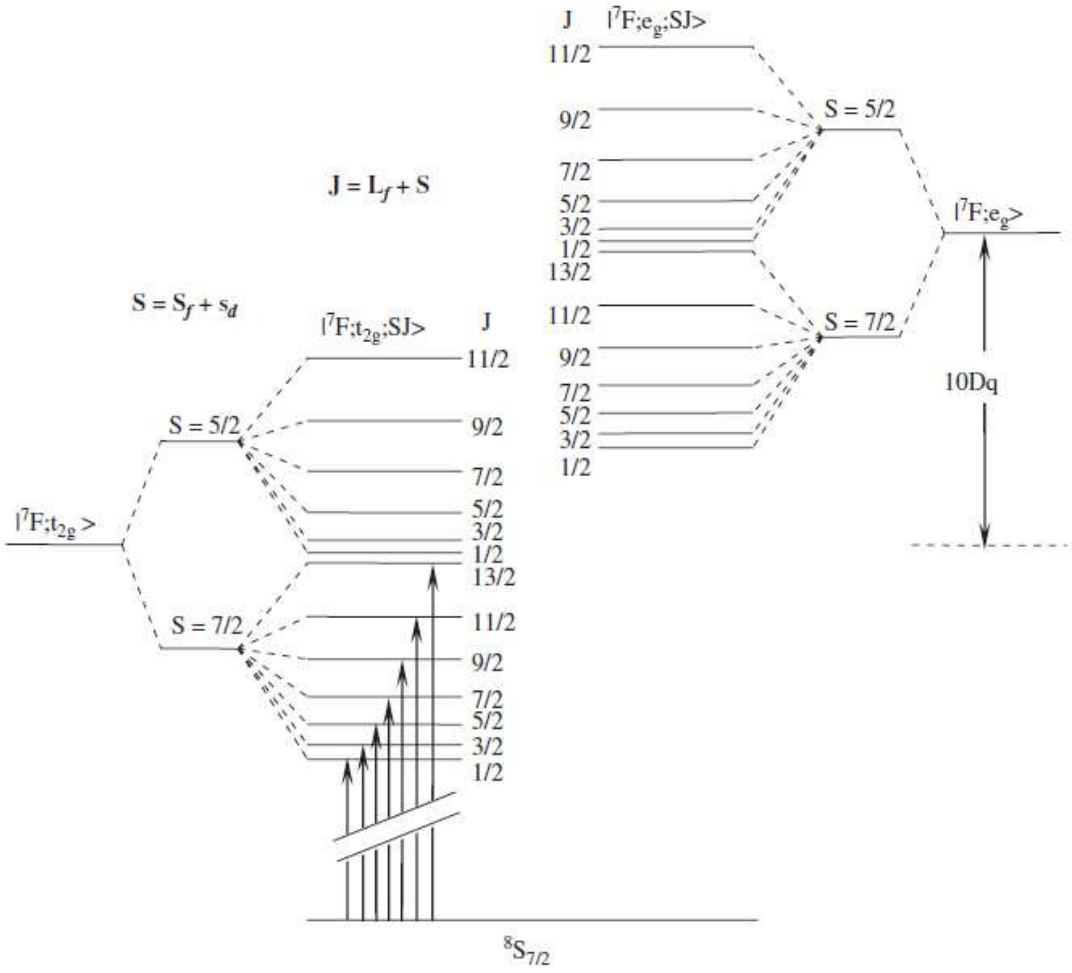

Figure 2.2: Schematic diagram of the Eu^{2+} energy levels within the $4f^6 5d$ configuration in an octahedral crystal field following the model proposed by Duan et. al. [27, 28]. S_f and L_f are the total spin and orbital quantum numbers of the f electrons and s_d is the spin of the d electron [29].

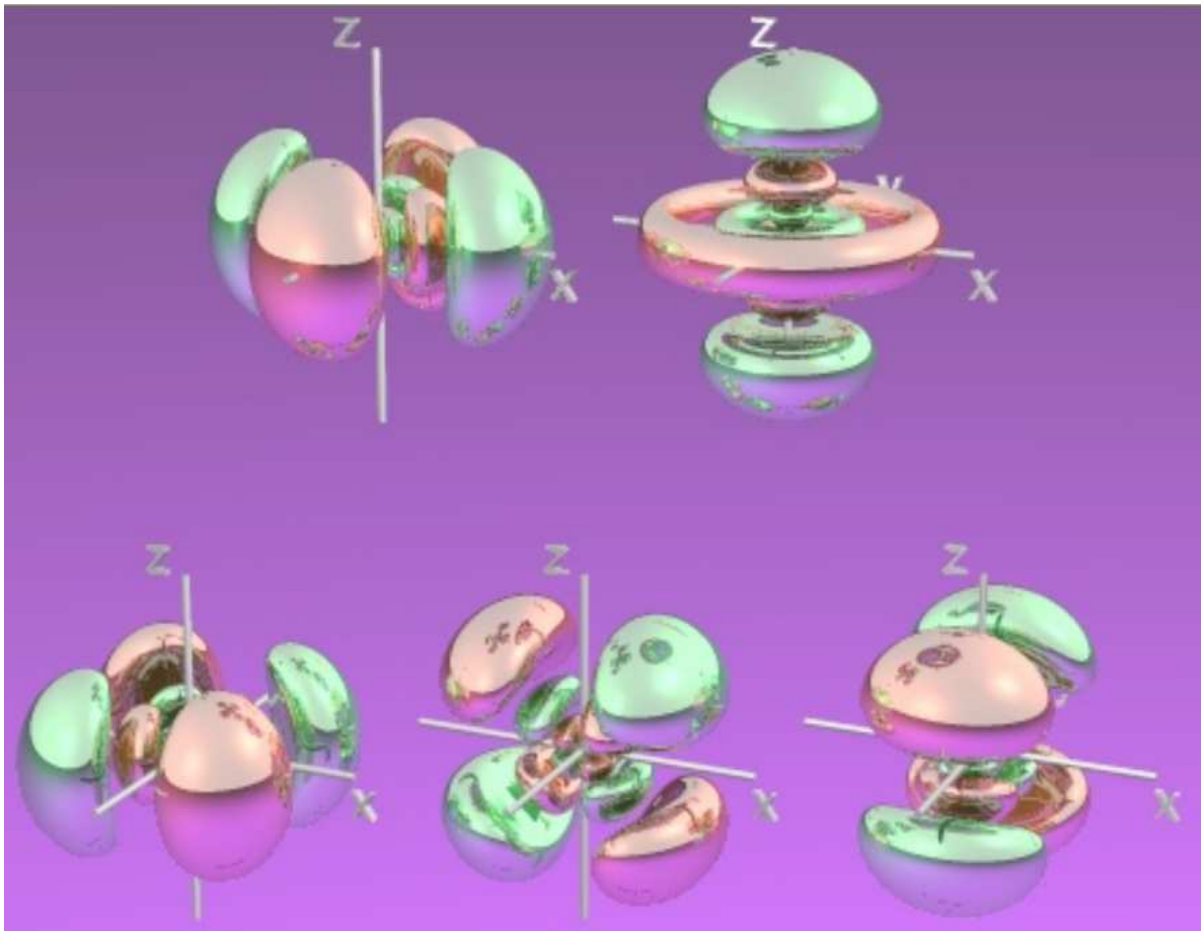

Figure 2.3: Schematic representation of the 5d electron orbitals. When located at an octahedrally coordinated center, the three lower orbitals in the picture are associated with the t_{2g} terms and are in a lower energy configuration than the two upper e_g terms. Image obtained from The Orbitron^{TM} online [30].

of the absorption spectra in first year chemistry and physics textbooks show spectra for low-pressure gas discharges, which are characterized by very sharp lines, the absorption spectra for condensed matter systems can be broad and very complex. The reasons have been stated in the sections on splitting and Hamiltonians.

A usual method for measuring absorption is to take a sample and send a known quanta (energy) of light through the sample having a thickness d. The transmission T coefficient is a measure of transmitted intensity, $I(\nu)$, (the intensity of light that the detector measures on the outgoing side of the sample) over the incident intensity, $I_o(\nu)$. The explicit equation for the transmission coefficient is $T = I(\nu)/I_o(\nu)$. Most modern spectrophotometers use beam splitters or chopped signals to measure both the incident and transmitted light simultaneously. This is done to both speed up measurements and to reduce the error associated with variation of source lamp intensity over time. One can use the transmission coefficient to find the optical density, $OD = \log_{10}(1/T)$. This relation can be used to find the absorption coefficient, $\alpha(\nu)$ by the relation

$$OD = \log_{10}(1/T) = \frac{\alpha(\nu)l}{ln(10)} \tag{2.11}$$

or more commonly known in the form of the Beer-Lambert law

$$I(\nu) = I_o(\nu)e^{-\alpha(\nu)l} \tag{2.12}$$

where where $I_o(\nu)$ is the intensity of the irradiation at frequency ν, $I(\nu)$ is the intensity of the transmitted radiation at frequency ν, l is the thickness of the sample, and $\alpha(\nu)$ is the corresponding absorption coefficient. A plot of the absorption coefficient versus the incident wavelength forms an absorption spectrum. Absorption spectra are most beneficial when attempting to measure the transitions that do not lead to photoemission.

2.3.2 Photoexcitation

Photoexcitation is a powerful technique involving the observation of a fixed frequency or frequencies of emission while actively scanning the incident, or exciting, frequency. In inorganic

solids, especially those doped with elements such as rare-earth or transition metals, there are usually many absorption bands that overlap and can completely wash out the details of a certain absorption center of interest. As an example, when magnesium oxide is doped with vanadium the defect ions are found to be both V^{2+} and V^{3+}. In magnesium oxide V^{2+} ions emit luminescence in the near infrared (900 nm). The absorption bands of V^{2+} ions are superimposed with and much weaker than the V^{3+} absorption bands and they cannot be detected with absorption measurements. However, with excitation spectroscopy, such measurements are possible because a strong emission at a particular excitation wavelength indicates that the material is absorbing strongly at that wavelength. Furthermore, phase sensitive detection is possible using lock-in amplifiers which allows one to distinguish between multiple absorbing optical centers provided that they have different radiative lifetimes. The equation for the photoexcitation intensity, $S(\nu)$, as it relates to the Beer-Lambert law is

$$S(\nu) = I_o(\nu)(1 - e^{-\alpha(\nu)l}) \tag{2.13}$$

if α is small, then we may Taylor expand the second term in Equation 2.13. This allows us to directly correlate the absorption coefficient to the photoemission intensity and obtain

$$S(\nu) \approx I_o(\nu)\alpha(\nu)l \tag{2.14}$$

The intensity measurements must be corrected for the efficiency of the apparatus, and this is usually done with a calibrated measuring instrument in a separate scan with all other parameters the same with exception that the sample is replaced with the measuring device.

2.3.3 Emission

Emission or photoemission is based on the radiative transition of an excited atomic electron to a lower energy state. In order to obtain a measurement of such a transition, the electron(s) must first be excited to some unoccupied level. This can be done in any number of ways. Today, lasers are a common tool employed in emission spectroscopy. While these solid state

and dye pumped lasers provide an intense source, there is also still considerable use for broad spectral range lamps that can be tuned to a given absorbing wavelength. In addition, light emitting diodes, LED's, have become relatively inexpensive even for some very short wavelengths ' that were once very rare. Not all wavelengths can be accessed by any one system. However, by choosing the appropriate light source the range from 193–2500 nm is well covered.

Once the solid is in the excited state it may have several relaxation channels. The radiative channel results in the emission of a photon (typically with a rate on the order of 10^8–$10^3 s^{-1}$). Non-radiative relaxations can result in even larger decay rates, leading in some cases to a complete quenching of the luminescence. In special cases, two photons may be absorbed in sequence followed by the emission of a photon with an energy higher than those of the absorbed photons - this is known as up-conversion. If two photons are absorbed simultaneously, the term two-photon absorption is used. In the converse, one photon may be absorbed and the level depopulate by a sequential emission of two photons which is known as quantum cutting. In this dissertation only the single absorbed/emitted photon case is observed. Two important terms that will be used later to describe this process are:

1. Stokes shift (ΔS): This is defined as the shift in energy between the emission and absorption band peaks [24].

2. Zero Phonon line (ZPL): This is described as the energy at which there are zero vibrational levels involved in the absorption/emission transition. The observed intensity of this line is directly related to the degree to which the optical center couples to the lattice. If there is no vibrational coupling and the sample temperature is low (so that relatively few ground state vibrational levels are accessible), all of the emission intensity will be contained in the zero phonon line and it will be a sharp peak. As coupling to the lattice increases, vibrational sidebands will appear on the low (high) energy side of the emission (absorption) and the intensity of the ZPL will decrease. As temperature

increases, sidebands appear on both sides of the ZPL. If the vibrational coupling is sufficiently large, then the ZPL does not appear [24].

Note: if the ground state and excited state parabola (as seen on a configurational coordinate diagram) have the same curvature, then ΔS is simply twice the absolute energy separation of either the emission or excitation peak from the ZPL (i.e. $\Delta S = 2 \times |E_{em} - E_{ZPL}|$).

2.4 The Staircase Spectra Observed in Some Eu^{2+} Compounds

In the detection of photoexcitation of divalent europium a characteristic staircase structure is commonly observed [31–36]. The staircase can be explained by the splitting of the ground state of the $4f^6$ core and the $5d$ electron assuming a weak or null Coulomb interaction, i.e., by transitions from the $^8S_{7/2}$ to the seven ^7F_J multiplets (J = 0-6) of the excited $4f^6(^7F_J)5d^1$ (t_{2g}) configuration [37]. The splitting of the J-multiplets is the result of the Coulomb interaction between the six 4f electrons and their spin-orbit coupling. The similarity between peak energy differences of this staircase structure and those of the $^7F_0$-$^7F_6$ for Eu^{3+} multiplets supports the validity of this model. Figure 2.4 is representative of a typical spectrum that demonstrates the staircase structure. The nature of $4f \leftrightarrow 4f$ transitions does not change much when changing the host lattice [38] which allows the approximate locations of the ^7F_J levels to be designated in the spectra.

2.5 References

[13] P. Dorenbos, J. Lumin., **91**, 91, (2000).

[14] P. Dorenbos, J. Phys.: Condens. Matter., **15**, 575, (2003).

[15] P. Dorenbos, J. Lumin., **108**, 301, (2004).

[16] P. Dorenbos, J. Phys.: Condens. Matter., **15**, 4797, (2003).

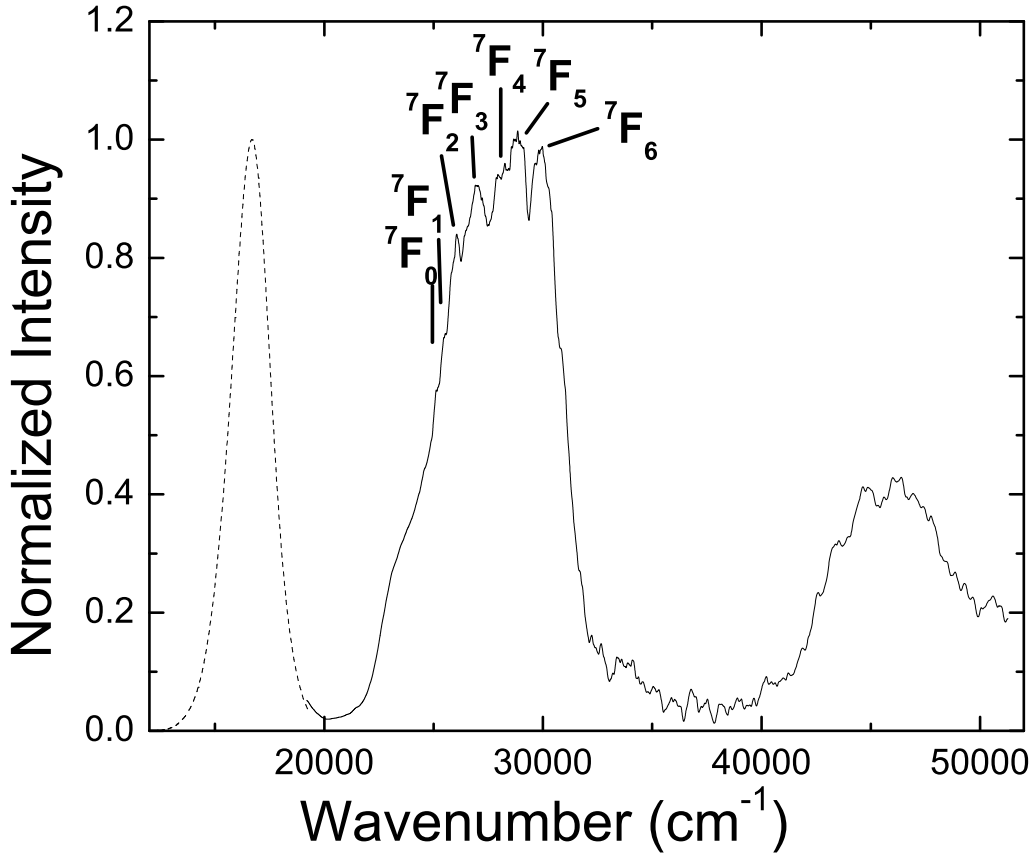

Figure 2.4: This image shows what is characteristic of a staircase in the excitation spectrum (solid curve) of divalent europium. Here the emission spectrum (dashed curve) is plotted as well. Generally, a broad peak (d level) is superimposed with up to seven ($5d4f$) major bands. Each of these levels can in turn split again in different manners according to the specific symmetry of the crystal field.

[17] P. Dorenbos, J. Andriessen, M. Marsman, and C.W.E. Van Eijk, Rad. Effects and Defects in Solids, **154**, 237, (2001).

[18] H. L. Schläfer and G. Gliemann, *Basic principles of ligand field theory*; translated from the German by D. F. Ilten., Wiley-Interscience, New York, (1969).

[19] M. Geller, Lecture Notes on Advanced Condensed Matter Physics, The University of Georgia, Athens, (2007).

[20] D.D. Vvedensky, Lecture Notes on Quantum Theory of Electrons in Solids, Imperial College, London, (2000).

[21] A. L. Fetter and J. D. Walecka, *Quantum Theory of Many-Particle Systems*, Dover Publications, Inc., Mineola, (2003).

[22] J. S. Griffith, *The Theory of Transition-Metal Ions*, Cambridge University Press, Cambridge, (1961).

[23] A. Haug, *Theoretical Solid State Physics*, Pergamon Press, Oxford, (1972).

[24] B. Henderson and G.F. Imbusch, *Optical Spectroscopy of Inorganic Solids*, Oxford University Press, Oxford, (1989).

[25] R.C. Gibbs,D.T. Wilber, and H.E. White, Phys. Rev. textbf29, 790 (1927).

[26] S. Sugano, Y. Tanabe, and H. Kamimura, *Multiplets of Transition-Metal Ions in Crystals.*, Academic Press, New York, (1970).

[27] C.K. Duan, M.F. Reid, and G.W. Burdick, Phys. Rev. B, **66**, 155108, (2002).

[28] C.K. Duan and M.F. Reid, J. Solid State Chem., **171**, 299, (2003).

[29] S. García-Revilla and R. Valiente, J. Phys.: Condens. Matter, **18**, 11139, (2006).

[30] M. Winter, The Orbitron: a gallery of orbitals on the WWW, WEB: http://winter.group.shef.ac.uk/orbitron/AOs/5d/index.html (2006).

[31] A.A. Kaplyanskii, P.P. Zakharchenya, Opt. i Spektrosk., **13**, 597, (1962).

[32] E. Loh, Phys. Rev., **175**, 533, (1968).

[33] B.M.C. Dujardin, C. Pedrini, J. Lumin. **54**, 259, (1993).

[34] G.W. Burdick, A. Burdick, V. Beev, Chang-Kui Duan, M.F. Reid, J. Lumin, **118**, 205, (2006).

[35] F. M. Ryan, W. Lehmann, D. W. Feldman, and J. Murphy, J. Electrochem. Soc., **121**, 1475, (1974).

[36] M. J. Freiser, S. Methfesskl, and F. Holtzberg, J. App. Phys., **39**, 900, (1968).

[37] P. Dorenbos, J. Phys.: Condens. Matter., **15**, 2645, (2003).

[38] J. Overmeyer and R. J. Gambino, Phys Lett., **9**, 108, (1964).

m	m'	$k=0$	$k=2$		$k=4$	
± 2	± 2	1	-2	$\times 1/7$	1	$\times 1/21$
± 2	∓ 2	0	0		$\sqrt{70}$	
± 2	± 1	0	$\sqrt{6}$		$-\sqrt{5}$	
± 2	∓ 1	0	0		$-\sqrt{35}$	
± 2	0	0	-2		$\sqrt{15}$	
± 1	± 1	1	1		-4	
± 1	∓ 1	0	$-\sqrt{6}$		$-\sqrt{40}$	
± 1	0	0	1		$\sqrt{30}$	
0	0	1	2		6	

Table 2.1: These are the relevant (i.e. non-zero) values of $c^k(lm, l'm') = (-1)^{m-m'} c^k(l'm', lm)$ for $l = l' = 2$. The values of c^k are non-zero only for $k = 0, 2, 4$

Chapter 3

Experimental Details

3.1 Sample preparation

Polycrystalline samples of $Cs_2(Ca_{0.99}Eu_{0.01})P_2O_7$ and $Cs_2(Sr_{0.99}Eu_{0.01})P_2O_7$ were synthesized by a classic solid-state reaction technique. The starting materials used were analytical grade Cs_2CO_3 (10 mole % excess) $CaCO_3$, $SrCO_3$ and $(NH_4)_2HPO_4$ (10 mole% excess) and Eu_2O_3. The samples were heated at 300° C for one hour in air and then heated twice at 800° C for 5 hrs in a slightly reducing atmosphere with intermediate grindings. In both materials, the XRD pattern confirmed the formation of phase pure material. Since the final products were found to be hygroscopic all optical measurements were carried out with the samples sealed in quartz tubes.

3.2 Emission

Similar techniques were used to measure the emission spectra of the $Cs_2M^{2+}P_2O_7$(M = Ca, Sr):Eu^{2+} samples. The emission spectra were measured over several excitation energies using multiple collection methods, and varying temperature regimes.

3.2.1 Excitation Sources

- 390 nm (375nm UV LED (Nitchia) with 390nm band pass filter full width half maximum 10 nm).
- 355 nm tripled Nd:YAG line (Spectra Physics).

3.2.2 Collection Methods

- UV/VIS liquid nitrogen cooled CCD (charge coupled device) camera (Princeton Instruments, LN/CCD512TKB). The camera is attached to a Spectra Pro® 275 single monochromator utilizing a 150 groove/mm grating blazed at 300 nm. The monochromator was driven by a Spectra Drive Stepping Motor scan controller. In order to cover the full range of emission, the monochromator was set to center wavelengths of 200, 400, and 600 nm. The pixels were calibrated using automated software controlling the driver. A 635 nm diode laser, a doubled Nd:YAG (532 nm), and the spectral lines (488, 514 nm) from an Ar ion laser were used to cross check the calibration. Data consisted typically of a 9 second integration time over a spectral range of 250 nm with a resolution of 0.5 nm/pixel. The spectra were collected with private software using a LabView 6.1 program and later combined in a graphical analysis software package after correcting for photon flux and pixel sensitivity. The input to the slits were coupled to a UV grade fiber optic cable and various appropriate lenses and filters were used to obtain one to one images of the sample luminescence onto the fiber entrance.

- VIS/NIR thermoelectrically cooled CCD (Kestrel Spec) to -20° C attached to a Spectra Pro® 275 single monochromator with 50 groove/mm grating blazed at 600 nm. The monochromator was driven by a Spectra Drive Stepping Motor scan controller. It was set to 550 nm and the pixels were calibrated using a 635 nm diode laser, a doubled Nd:YAG (532 nm), and the spectral lines (488, 514 nm) from an Ar ion laser. Data were colected during 10 second integration times over a spectral range of 300 nm with a resolution of $\sim$ 0.5 nm/pixel. The spectra were collected with manufacturer software and later combined with the excitation data in a graphical analysis software package after correcting for photon flux and pixel sensitivity. The input to the slits were coupled to a UV grade fiber optic cable and various appropriate lenses and filters were used to obtain one to one images of the sample luminescence onto the fiber entrance.

3.2.3 Sample Preparation and Temperature Handling

- Low temperature measurements (10 and 80 K) were obtained by placing the samples in one of two commercially available flow through cryostats, an Oxford Instruments Optistat LT continuous flow cryostat and an Oxford Instruments flow-through cryostat that has been custom modified to perform both emission measurements and excitation measurements at LH (liquid Helium) temperatures. The major modification consists of a mounting sleeve that will couple to the Cary-14 Spectrophotometer. All reported data at 10 K were done in this "Cary" cryostat.

- Room temperature emission was collected in open air with custom built sample holders for the quartz tube sample holders. No special equipment was necessary.

- High temperature measurements were carried out in a high temperature furnace with the samples in a custom built sample holder and in a nitrogen buffer atmosphere. The temperature was controlled with an Omega temperature controller custom modified to meet the requirements of the furnace.

3.3 Excitation

Excitation spectra were recorded in a modified Cary 14 spectrophotometer, using the chopped radiation of deuterium and tungsten lamps as excitation sources. The sample was placed into an Oxford Instruments flow-through cryostat, located in the sample chamber of the spectrophotometer. Luminescence was observed at right angles with a Hamamatsu R212 photomultiplier tube (PMT), the detection wavelength was determined by narrow band interference filters at multiple regions of interest that will be indicated on the presented figures. To increase the signal to noise ratio and to suppress the dark current of the PMT, the signal was processed with a Stanford Research Systems model SR 830 DSP lock-in amplifier. The excitation spectra were corrected for excitation photon flux using a calibrated Hamamatsu photodiode as reference detector. By using the lock-in-amplifier we are further

able to deduce the relative phase of emission from different active centers in the host crystal. This technique was mentioned in section 2.3.2. For example, with the lock-in auto-phased to the reflected lamp light where the x-component signal is "zeroed" (to within the noise limit) it is possible to see the lagging out of phase emission of Eu^{3+}. This shows up in the spectra as a negative signal for the x-component. See Figure 3.1.

3.4 Lifetime: Time Resolved Spectroscopy Measurements

For relaxation time measurements, the samples were again placed into the Oxford Instruments flow-through cryostat and illuminated with the pulsed radiation of an UV light emitting diode (LED) at an emission maximum of 375 nm, which matches the energetically lowest absorption peak of the phosphor. The LED was driven at a repetition rate of 1 MHz with the output of an Avtech AVP-C pulse generator, boosted by a high frequency Avantech power amplifier. The pulse width of the LED was measured to be 2 ns. Luminescence was detected at a right angle with a Hamamatsu R212 PMT, attached to the cryostat via a light tight tube; an interference filter (center wavelength 560 nm, 10 nm bandwidth for Sr, or 580 nm, 10 nm bandwidth for Ca) was inserted in the detection path and determined the detection wavelength. In order to avoid room light from entering the system, the excitation window of the cryostat was covered with a Schott UG-11 filter that transmits the LED radiation, but blocks at wavelengths of > 400 nm. The PMT signal was counted using an Ortec 567 time-to-amplitude converter with output to a computer and commercial counting software to obtain the decay profiles of the divalent europium emission. The temporal resolution of the setup, including the pulsed LED, was 2 ns.

A second set of measurements included high temperature measurements of lifetime (up to 800 K). This required a high temperature furnace with custom quartz tube built for such measurements. A 375 nm LED was used as the excitation source and a dichroic filter with selective bandpass properties at 0 and 45 degree incidence angle was used to both focus the excitation source onto the sample and the emitted light onto the slits of a monochromator

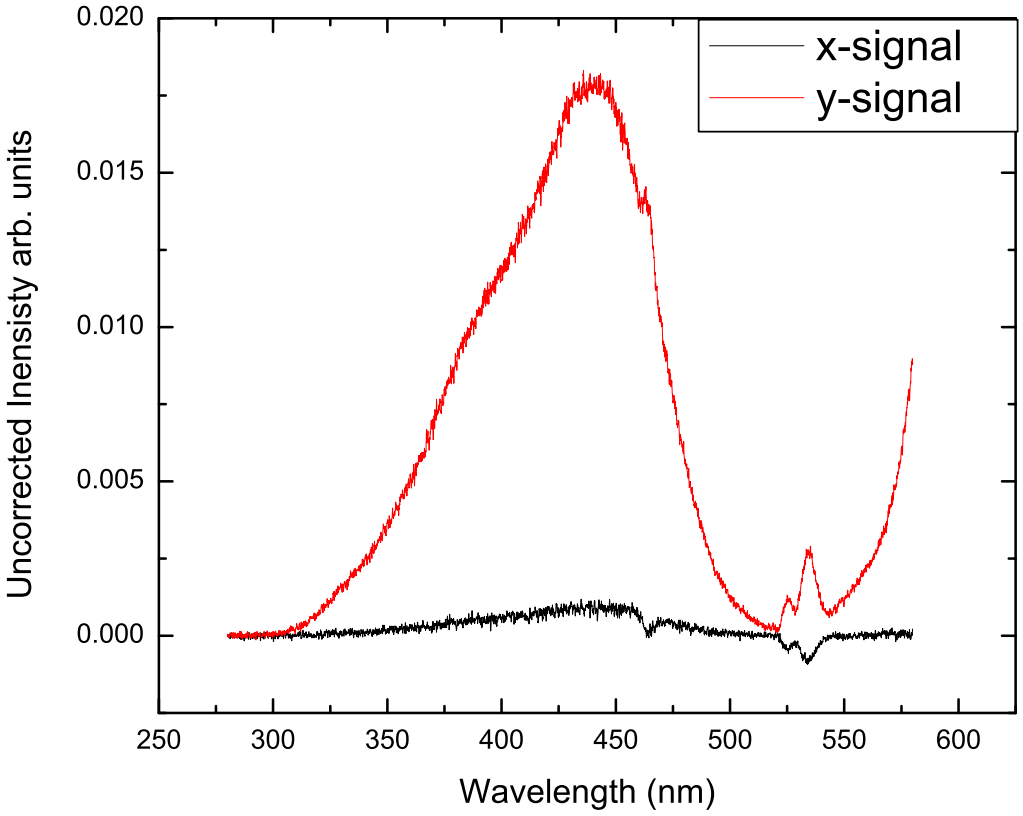

Figure 3.1: This is an example of both the in-phase and out of phase components of the Photoluminescent Excitation Spectra of $Cs_2CaP_2O_7$:Eu^{2+}. The out of phase signal is associated with Eu^{3+} impurities.

with a Hamamatsu R212 PMT attached to the exit slit. The detection wavelengths were determined by the monochromator and set to 560 nm for Sr, and 580 nm for Ca. The PMT signal was recorded with a photon counting system, using an Ortec 567 time-to-amplitude converter with output to a computer and custom counting software to obtain the decay profiles of the divalent europium emission. The temporal resolution of the setup, including the pulsed LED, was 2 ns.

Chapter 4

Experimental Results and Parameter Determinations

4.1 The $Cs_2M^{2+}P_2O_7$(M = Ca, Sr) Crystal Structure

4.1.1 X-Ray Diffraction

The diffraction measurements were performed on a powder X-ray spectrograph at GE global research. The diffraction pattern of $Cs_2CaP_2O_7$:Eu^{2+} is presented in Figure 4.1. The diffraction pattern for $Cs_2SrP_2O_7$:Eu^{2+} was also collected, but is not presented. There is good agreement with the previously reported structures when the two patterns are compared with that of the undoped $Cs_2SrP_2O_7$ and $Cs_2CaP_2O_7$ [39].

4.1.2 Crystal Structure

The crystal structure has been determined for both samples from the XRD data that of $Cs_2SrP_2O_7$ is shown in Figure 4.2. Included in the figure is a stereographic view of the compound. The basic monoclinic unit cell has dimensions: $a = 10.528$Å, $b = 6.081$Å, $c = 14.766$Å, $\alpha = 90°$, $\beta = 118.3°$, and, $\gamma = 90°$. This overall structure contains isolated octahedra of $[SrO_6]$ and bi-tetrahedra $[P_2O_7]$ groups. These two groups share their oxygen vertices and form a rigid, infinitely repeating structure of $[SrP_2O_7]^{2-}$. This anionic sublattice is characterized by infinite hexagonal tunnels where the Cesium atoms reside. The Cesium atoms are located off center in these tunnels and are close to the walls. They sit in an environment that is twelve coordinated with Oxygen atoms using a cutoff distance of 3.6 Å. The Sr-O bond lengths in the octahedra are 238 pm(2×), 247 pm(2×), and 263 pm(2×) in the x, y, and z directions respectively and 2× indicates that there are two atoms located at that distance.

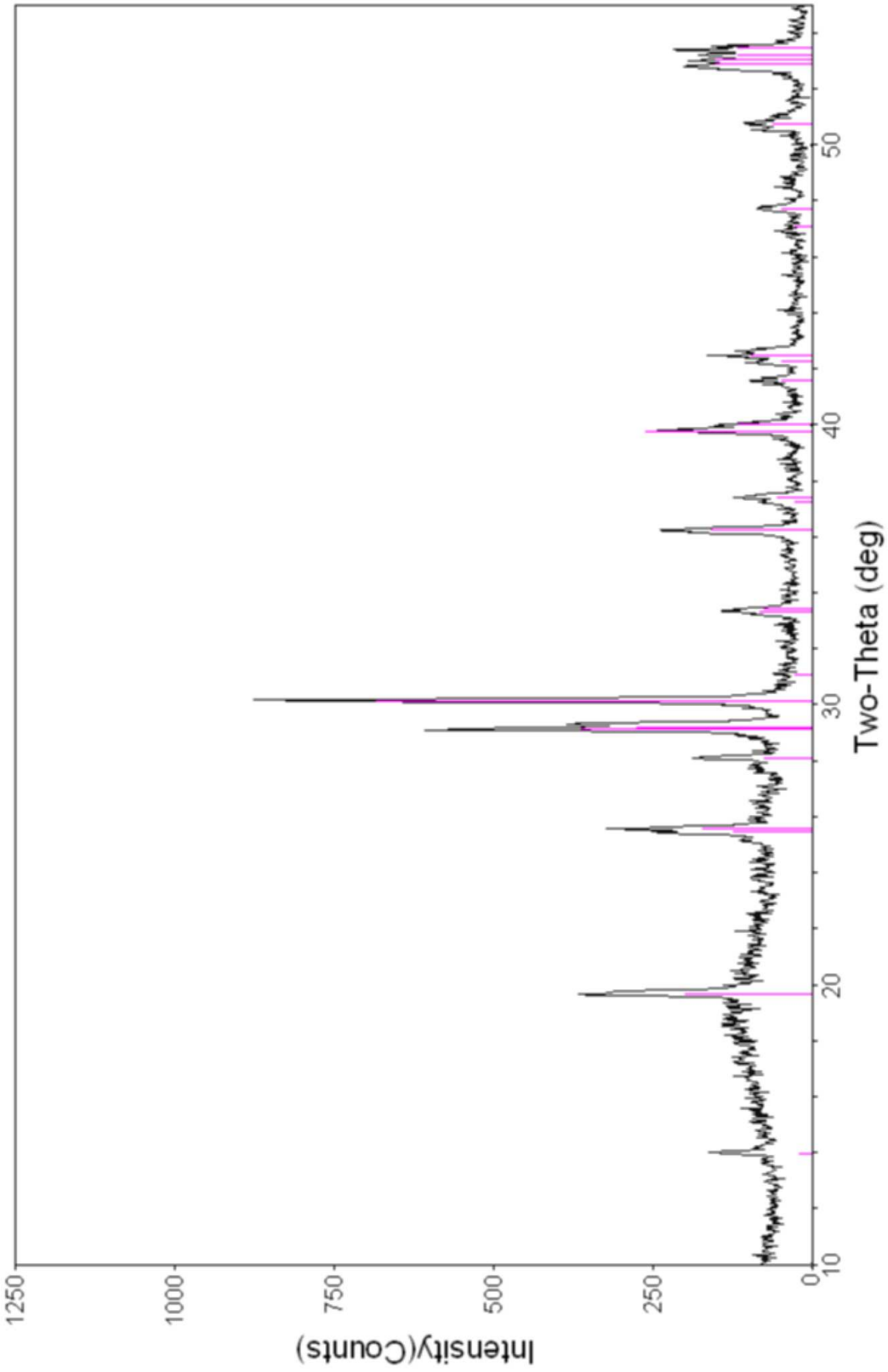

Figure 4.1: X-ray diffraction data obtained from GE Global Research for $Cs_2CaP_2O_7$:Eu^{2+}.

The O-Sr-O bond angles deviate only slightly from 90° to within a few degrees. Eu^{2+} substitutively replaces the strontium atoms as an impurity and the octahedrally coordinated Eu^{2+} ion forms the optically active center.

Similarly, the structure for pure $Cs_2CaP_2O_7$ crystals has been determined by Zatovsky et al [40]. The crystal cell parameters are $a = 10.261$Å, $b = 5.9316$Å, $c = 14.4808$Å, $\alpha = 90°$, $\beta = 118.54°$, and $\gamma = 90°$. The overall structure is the same including the isolated octahedra of $[CaO_6]$ and bi-tetrahedra $[P_2O_7]$ groups. Cesium atoms occupy the hexagonal tunnels in the same manner also. There is increased symmetry in the Ca-O bond lengths at 236 pm(2×), 236 pm(2×), and 263 pm(2×) in the x, y, and z directions respectively. The O-Ca-O bond angles also deviate only slightly from 90° to within a few degrees. Fourier Transform Infra-red measurements (FTIR) have been performed on these structures by Zatovsky [40] in order to determine the phonon frequencies for the lattice vibrations and there are numerous bands within the range of 200 to 1200 cm^{-1} which is consistent with other double diphosphates. These bands have been attributed to the many phosphate groups, P-O-P bands, and O-P bands within the crystal and should provide a large band width at the peak emission and absorption frequencies [41–44]. These structures provide near perfect octahedral symmetry for the strontium and calcium sites.

4.2 Excitation

The combined emission and excitation spectra for $Cs_2CaP_2O_7$:Eu^{2+}, and $Cs_2SrP_2O_7$:Eu^{2+} are represented in Figures 4.3 and 4.4. The excitation bands can be assigned in the usual manner for a defect in an octahedral symmetry. The high energy bands are those emanating from the $4f^7[^8S_{7/2}] \rightarrow 4f^6 5d^1[e_g]$ and is located between 40,000–50,000 cm^{-1} for both samples. The low energy bands are those emanating from the $4f^7[^8S_{7/2}] \rightarrow 4f^6 5d^1[t_{2g}]$ and is located roughly for both samples between 21,000–35,000 cm^{-1}. The high energy (e_g) bands show signs of very slight splitting of the d_{z^2} and $d_{x^2-y^2}$ levels. The low energy bands are very interesting and exhibit a characteristic staircase structure. Each step in the t_{2g} bands is

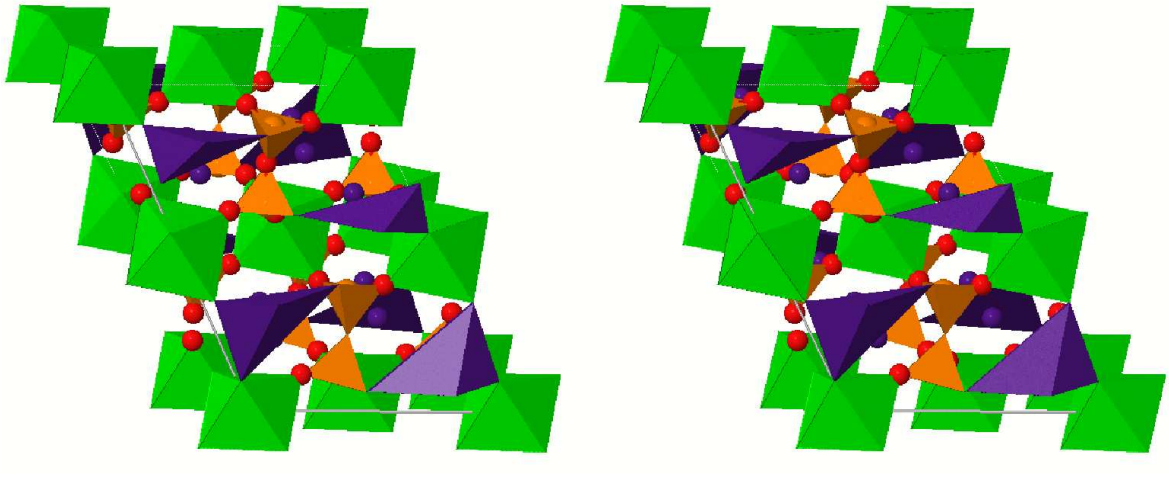

(a)

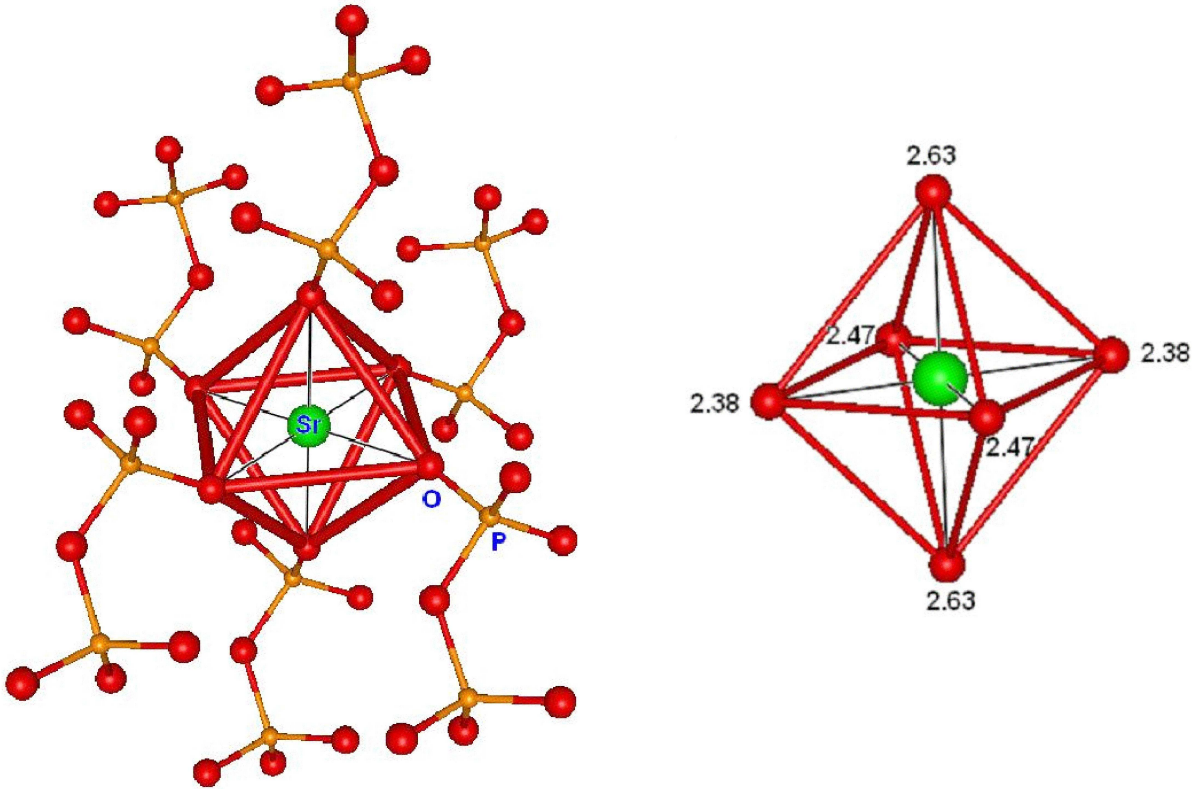

(b)

Figure 4.2: (a)Stereographic image of the crystal structure for $Cs_2Sr^{2+}P_2O_7$. To view it in 3-D simply cross your eyes and allow the middle image to come into focus. (b) At left is a blowup of the inner strontium atom with the attached pyrophosphates and at right is the inner octahedron with the bond lengths labeled. Used with permission [39].

indicative of a specific transfer from one of the ${}^7\mathrm{F}_J(J = 0 - 6)$ multiplets. The bands in Figures 4.3 and 4.4 have been assigned based on the free ion energies of Eu^{3+} given in [45]. These free ion energies will be close to those found in $Cs_2CaP_2O_7$ and $Cs_2SrP_2O_7$ because the $4f$ electrons are only weakly influenced by the crystal field. The highest ${}^7\mathrm{F}_6$ band is approximately assigned to the highest step in the staircase and based on the relative shifts between the remaining ${}^7\mathrm{F}_J(J \neq 6)$ levels all remaining levels are assigned. There is general agreement between the barycenters of each multiplet and the reported energy barycenters in the literature.

The crystal field splitting, $10Dq$, is determined by calculating the difference between the t_{2g} and e_g states. The centers of gravity ($CG's$) or centroids . for these peaks were calculated by the method of moments as described in [46]. First, the zeroth order moment, M_o is defined as the area under the emission or excitation band.

$$M_o = \int I(\nu)d\nu \tag{4.1}$$

where $I(\nu)$ is the intensity of the band as a function of wavenumber ν. The integral is performed over the domain of each band of interest. Next, the center of gravity is obtained by computing the first moment defined by

$$CG = M_1 = \frac{1}{M_o}\int I(\nu)\nu d\nu. \tag{4.2}$$

The second moment is defined as

$$M_2 = \frac{1}{M_o}\int I(\nu)(\nu - CG)^2 d\nu \tag{4.3}$$

from which the standard deviation, σ, from the centroid may be obtained upon taking the square root of M_2.

The $10Dq$, centroids for t_{2g} and e_g ($CG^{t_{2g}}, CG^{e_g}$), and the standard deviation ($\sigma^{t_{2g}}, \sigma^{e_g}$)are compiled in Table 4.2

A larger $10Dq$ in $Cs_2CaP_2O_7$:Eu^{2+} relative to $Cs_2SrP_2O_7$:Eu^{2+} is expected due to the smaller average $\langle Eu^{2+}–O^{2-}\rangle$ bond distance in the calcium material. This is observed in the

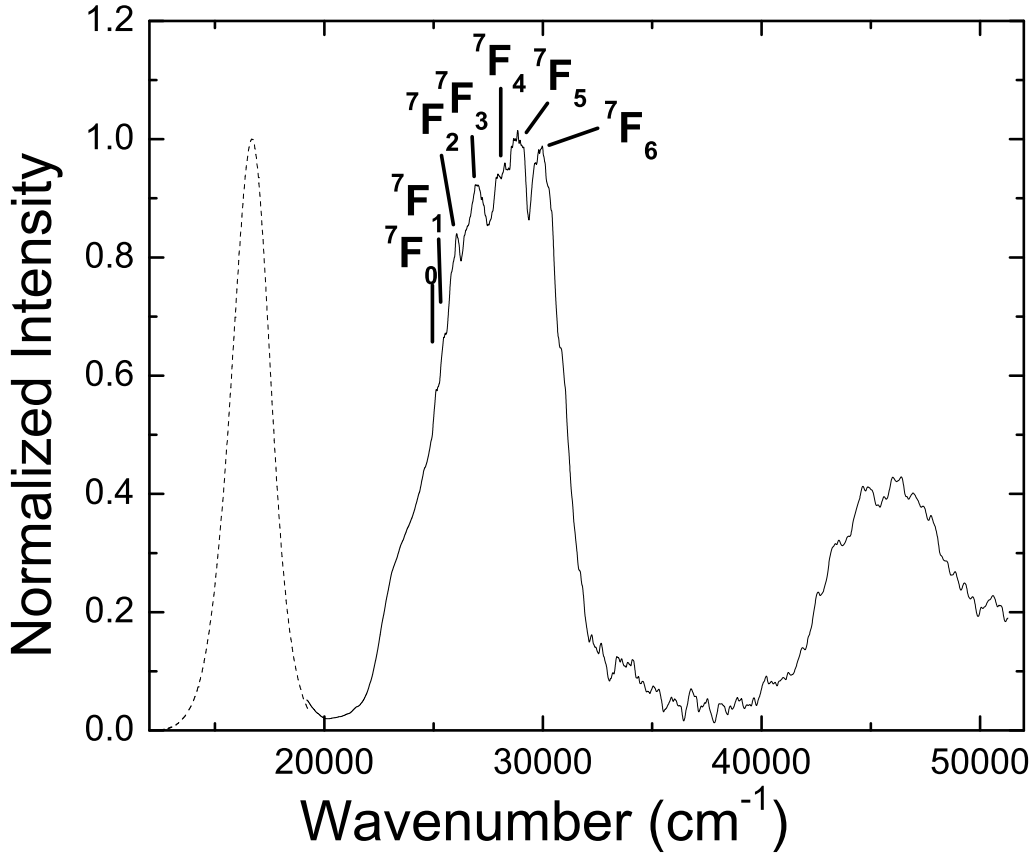

Figure 4.3: Emission (dashed line $\lambda_{ex} = 375$ nm)and excitation (dashed line $\lambda_{em} = 600$ nm) spectra for $Cs_2CaP_2O_7$:Eu^{2+} at 80 K. The locations of the ^7F_J levels are approximated.

Phosphor	$CG^{t_{2g}}$	CG^{e_g}	$10Dq$	$\sigma^{t_{2g}}$	σ^{e_g}
$Cs_2CaP_2O_7$:Eu^{2+}	27725	46183	18458	2619	3106
$Cs_2SrP_2O_7$:Eu^{2+}	28605	45381	17113	2512	2884

Table 4.1: The center of gravity of the $4f^6 5d^1(t_{2g})[CG^{t_{2g}}]$ and $4f^6 5d^1(e_g)[CG^{e_g}]$ electronic configurations, crystal field splitting ($10Dq$) and the standard deviation of the $t_{2g}[\sigma^{t_{2g}}]$ and $e_g[\sigma^{e_g}]$ excitation bands at $T = 80$ K; all values in cm^{-1}

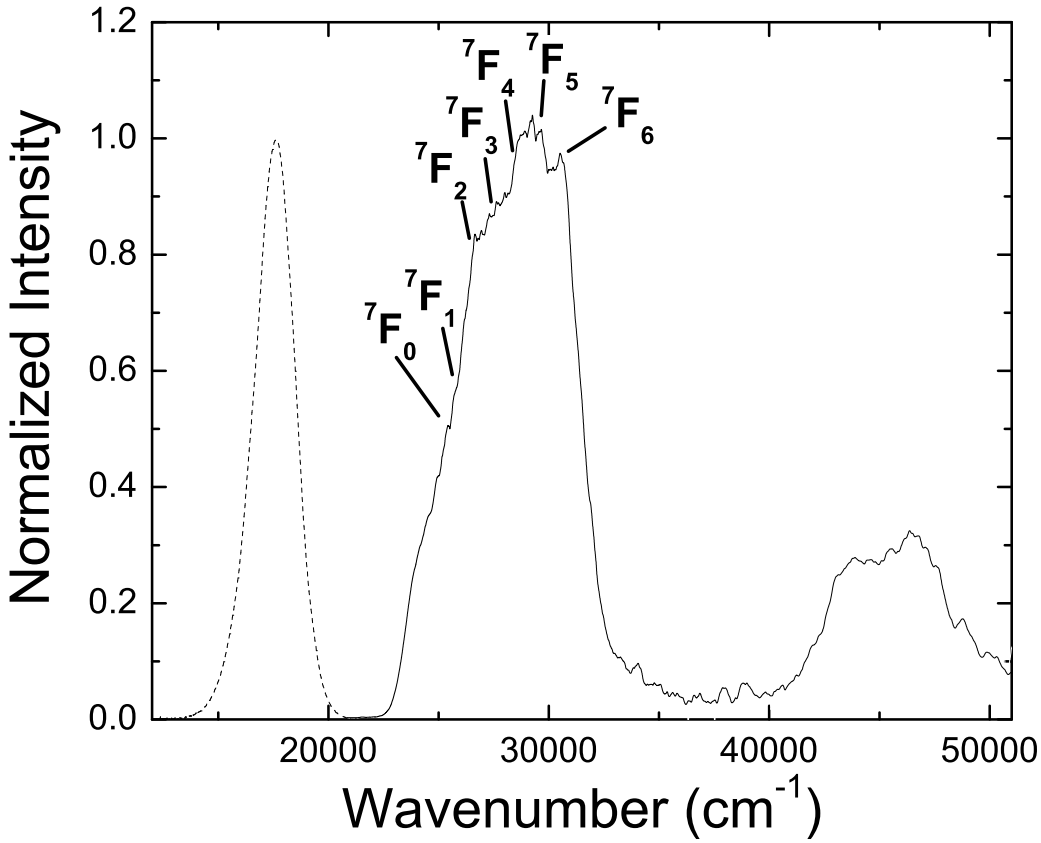

Figure 4.4: Emission (dashed line $\lambda_{ex} = 375$ nm)and excitation (dashed line $\lambda_{em} = 600$ nm) spectra for $Cs_2SrP_2O_7$:Eu^{2+} at 80 K. The locations of the ^7F_J levels are approximated.

experimental data. The larger $10Dq$ for $Cs_2CaP_2O_7$ is accounted for by the defect Eu^{2+} ion occupying a smaller Ca^{2+} ion site. This substitution causes the octahedral site to deform in order to accommodate the larger Eu^{2+} ion [47, 48]. Upon excitation, the $\langle Eu^{2+}–O^{2-}\rangle$ bond distance decreases for t_{2g} and increases for e_g.

4.3 Emission

The emission data have been analyzed for peak location and full width half maximum intensity, FWHM= Γ^{em}. Because the emission bands are approximately Gaussian, the second moment can be related to the FWHM by the relation

$$\Gamma^{em} = \sqrt{8 \ln 2 M_2}. \tag{4.4}$$

The emission spectrum of Eu^{2+} activated $Cs_2CaP_2O_7$:Eu^{2+} and $Cs_2CaP_2O_7$:Eu^{2+} is a broad symmetrical band centered at 607 nm (16 474 cm^{-1}) and 563 nm (17 762 cm^{-1}) with full width at half peak intensity (Γ^{em}) of 2191 cm^{-1} and 2147 cm^{-1}, respectively (Figures 4.3 and 4.4; Table 4.3). The phonon energy, $\hbar\omega$, and the Huang-Rhys parameter, S, may be calculated from the moments of the emission peaks. The phonon energies are 236 cm^{-1} for $Cs_2CaP_2O_7$ and 248 cm^{-1} for $Cs_2SrP_2O_7$. The S values represent the strength of the coupling of the excited state to the vibrating lattice. A value of $S = 0$ would represent no vibrational coupling and values of $S \geq 10$ would be large coupling. The S values calculated here are 18, and 17 for the calcium and strontium samples respectively which indicate a very strong coupling to the octahedral ligands.

The key features of the Eu^{2+} luminescence in both the calcium and strontium samples are the energetic locations of the two emission peaks. Both are at unusually long wavelengths which are not generally supported by divalent europium ions in phosphate materials. Specifically, $Cs_2CaP_2O_7$:Eu^{2+} is well into the orange at 600 nm and $Cs_2SrP_2O_7$:Eu^{2+} is yellow at 560 nm. Based on all known available data and a thorough literature search [49], these emissions are at the lowest ever observed in a Eu^{2+} doped phosphate based material.

4.4 The Stokes Shift (ΔS)

The Stokes shift is defined as the absolute energy difference between the emission and excitation maxima

$$\Delta S = |E^{em} - E^{ex}|. \tag{4.5}$$

The values E^{ex} and ΔS are listed in Table 4.3. The Stokes shifts for both samples are ≈ 1 eV. Ideally, the ZPL would be determined experimentally, by reaching a low enough temperature that a very sharp and narrow peak on both the excitation and emission data would be present and converge at the ZPL energy (E^{ZPL}). We did not see such a line. This result is anticipated due to the strong coupling constants for both compounds. Another, less accurate, method for determining ΔS that has been reported [50] is by first determining the position of the Zero Phonon Line. If the energy bands are symmetric, then ΔS is simply twice the energy difference of E^{ZPL} and E^{em} (the emission peak energy). If the bands are asymmetric, as is the case with these samples, then this method is invalid. Instead, the ZPL was determined by using three different methods. The first method is that of taking E^{ZPL} to be located at a position between 10-15% of the maximum intensity of the excitation spectrum. Second, is to approximate E^{ZPL} to be located at the point of intersection of the excitation and emission curves. The third method that was employed was to determine the onset of emission as an upper energy bound and the onset of excitation as a lower energy bound and averaging the two values. The E^{ZPL} obtained from all methods reasonably agree to within 100 to 200 cm^{-1} and the values using method three are reported in Table 4.3. Ultimately, because of the asymmetry and the uncertainty in the location of the lowest excitation band, the Stokes shift was determined by the equation

$$\Delta S = 2 \times |E^{ZPL} - E^{em}|. \tag{4.6}$$

In the literature, the most frequent, or average value, for the Stokes shift of Eu^{2+} in solids is reported to be 1350 cm^{-1} (0.16 eV)[49]. The values of the Stokes shift that we obtained are on the order of one electron volt in the $Cs_2M^{2+}P_2O_7$:Eu^{2+} materials which are extremely

large compared to the reported values. The reasons for this extremely large Stokes shift will be examined shortly.

4.5 Lifetime: Temperature Dependence, and Quenching

Time resolved spectroscopy measures the rate of change in the population of these electrons. The rate of relaxation of the excited electrons to the ground state is a function of the total number of excited electrons and their transition probability. If there is only one emission center then the relaxation rate decreases exponentially over time as the number of electrons in the excited state decreases.

Lifetime curves were collected every 25 K and then the characteristic lifetimes were determined by use of a graphical data analysis program. All of the data that were collected for both samples were shown to be of single exponential character. Lifetime data for both $Cs_2CaP_2O_7$:Eu^{2+} and $Cs_2SrP_2O_7$:Eu^{2+} at three different temperatures are shown in Figures 4.5 and 4.6. The decay times were determined at each temperature by fitting of a single exponential decay curve of the form

$$N = c + N(t_o)e^{-\frac{(t-t_o)}{\tau}} \tag{4.7}$$

where N is the number of photon counts observed at time t, c is a constant background factor, t_o is the initial start of decay, $N(t_o)$ is the number of counts at t_o (amplitude), and τ is the lifetime of emission.

The lifetime of the Eu^{2+} emission and in general for any luminescent center is temperature dependent. As the temperature rises one can expect that at some critical temperature the lifetime of the emission will begin to decrease and upon further heating reach a temperature at which it no longer radiates. The temperature dependence of the emission lifetimes of $Cs_2CaP_2O_7$ and $Cs_2SrP_2O_7$ are shown in figures 4.7 and 4.8. The lifetime at any temperature, $\tau(T)$, is given by the equation

$$\frac{1}{\tau(T)} = \frac{1}{\tau_o} + \frac{1}{\tau_{NR}} \tag{4.8}$$

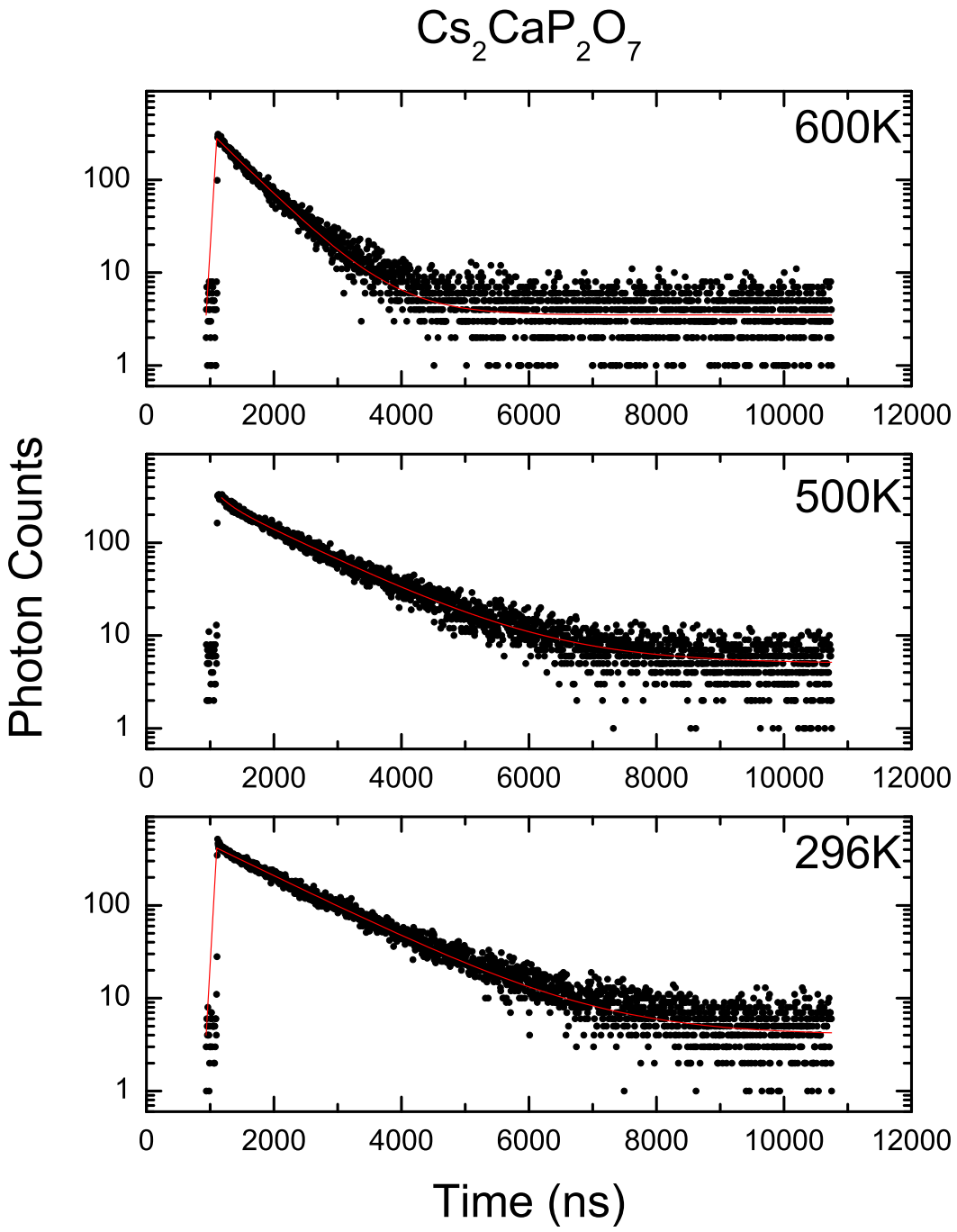

Figure 4.5: Characteristic lifetime data for $Cs_2CaP_2O_7$:Eu^{2+} at three different temperatures. The red curves are the single exponential curve fits to the data.

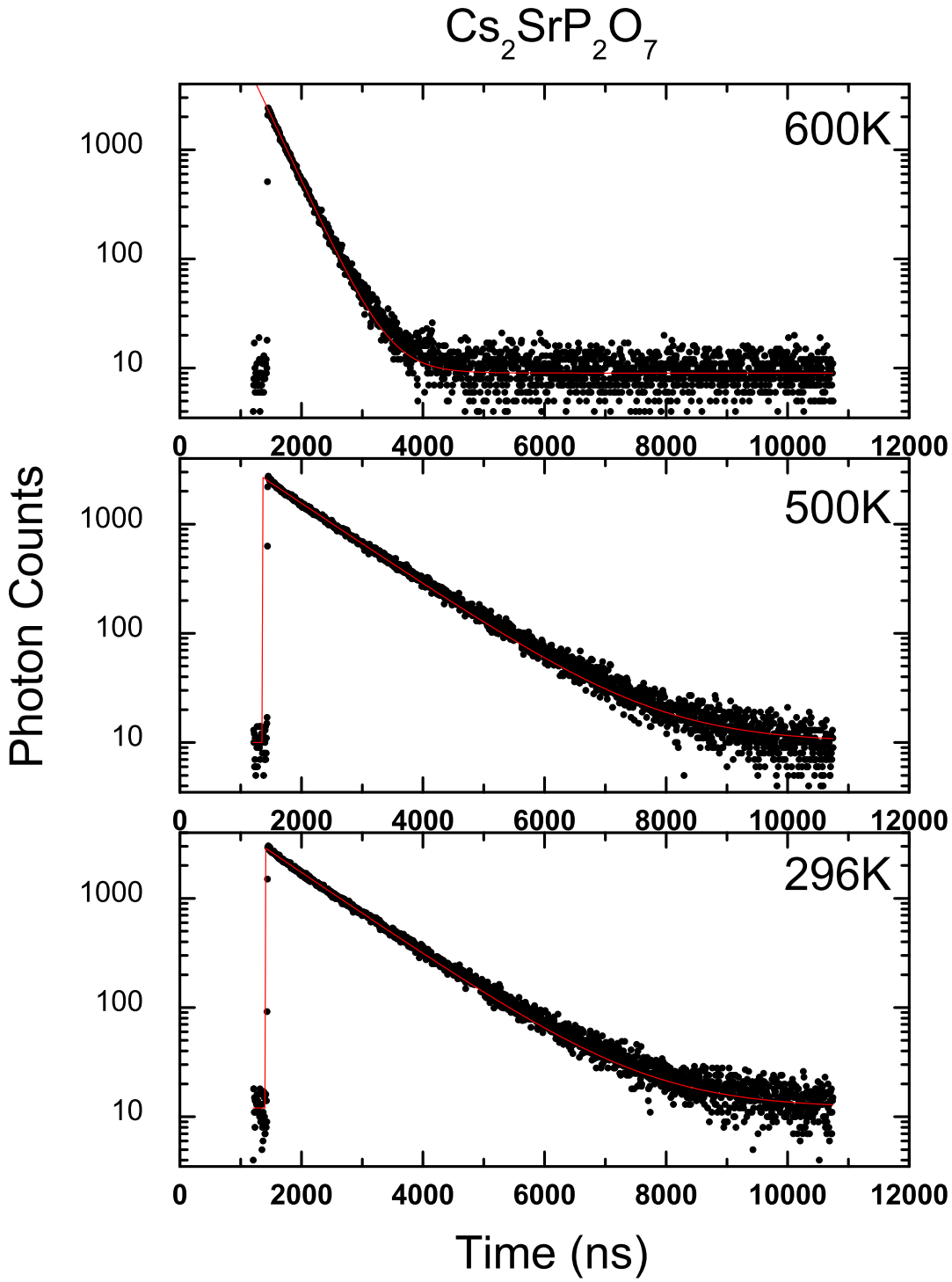

Figure 4.6: Characteristic lifetime data for $Cs_2SrP_2O_7$:Eu^{2+} at three different temperatures. The red curves are the single exponential curve fits to the data.

where τ_o is the zero temperature radiative lifetime, and τ_{NR} is the non-radiative lifetime. The data were fitted to the above equation by assuming that τ_{NR} varies following an Arrhenius law:

$$\frac{1}{\tau_{NR}} = Ae^{-\frac{\Delta E}{kT}} \tag{4.9}$$

where k is the Boltzmann constant, ΔE is the activation energy of thermal quenching, and A is a constant. The red curves in figures 4.7 and 4.8 are the best fit curves from equation 4.8. The temperature at which the lifetime has reached half of its initial value is defined as the quenching temperature $T_{0.5}$. From the best fit curves, the values are $\tau_o = 1.2$ μs and 1.3 μs, $\tau_{NR} = 1.2 \times 10^{-14}$ s and 7.14×10^{-15} s, $\Delta E = 7394$ cm^{-1} and 7900 cm^{-1}, and $T_{0.5} \approx 600$ K and 600 K for the $Cs_2CaP_2O_7$ and $Cs_2SrP_2O_7$ materials respectively. These values are compiled in Table 4.5.

The radiative lifetime of approximately 1.2 μs in both materials is consistent with the average reported lifetime for normal Eu^{2+} emission. The values of both $T_{0.5}$ and ΔE are very high in $Cs_2CaP_2O_7$:Eu^{2+} and $Cs_2SrP_2O_7$:Eu^{2+}. The normal quenching temperatures are usually between 100 and 300 K [49].

Dorenbos has attributed the thermal quenching to one main mechanism in Eu^{2+} containing material. It is the transfer of an electron from the lowest state of the relaxed Eu^{2+} $4f^6 5d^1$ electronic configuration to the host lattice conduction band states [51]. The normal idea of a configurational coordinate diagram must be modified in order to account for the idea of thermal quenching due to level crossing in Eu^{2+} containing solids. Therefore, the activation energy is more appropriately thought of as the energy required to raise the electron from the relaxed excited state into the host lattice conduction band. Due to this, there may not be a direct relation between the Stokes shift and the quenching temperature.

The high quenching temperature of the Eu^{2+} emission in $Cs_2CaP_2O_7$:Eu^{2+} and $Cs_2SrP_2O_7$:Eu^{2+} indicates that the lowest energy state of the relaxed Eu^{2+} $4f^6 5d^1$ electronic configuration is well isolated from the host lattice conduction band. A high quenching temperature has also

Phosphor	E^{ex}	E^{em}	Γ^{em}	$D(2+,A)$	ϵ_c	E^{ZPL}	ΔS	$\hbar\omega$	S
$Cs_2CaP_2O_7$:Eu^{2+}	25029	16583	2361	9000	4517	20833	8446	236	18
$Cs_2SrP_2O_7$:Eu^{2+}	25655	17475	2394	8381	4194	21645	8180	248	17

Table 4.2: Peak energy of the $4f^7$ $4f^6$ $[^7F_0]5d^1$ excitation transition E^{ex}, peak energy of emission band E^{em}, full width at half peak intensity of the emission band Γ^{em}, the red shift $D(2+,A)$, centroid shift ϵ_c ,energy of the zero phonon line E^{ZPL} the stokes shift $\Delta S = E^{ex}$-E^{em}, the calculated phonon energy $\hbar\omega$, and the Huang-Rhys parameter S; all values in cm^{-1} (except S which is unitless) and at T= 80 K.

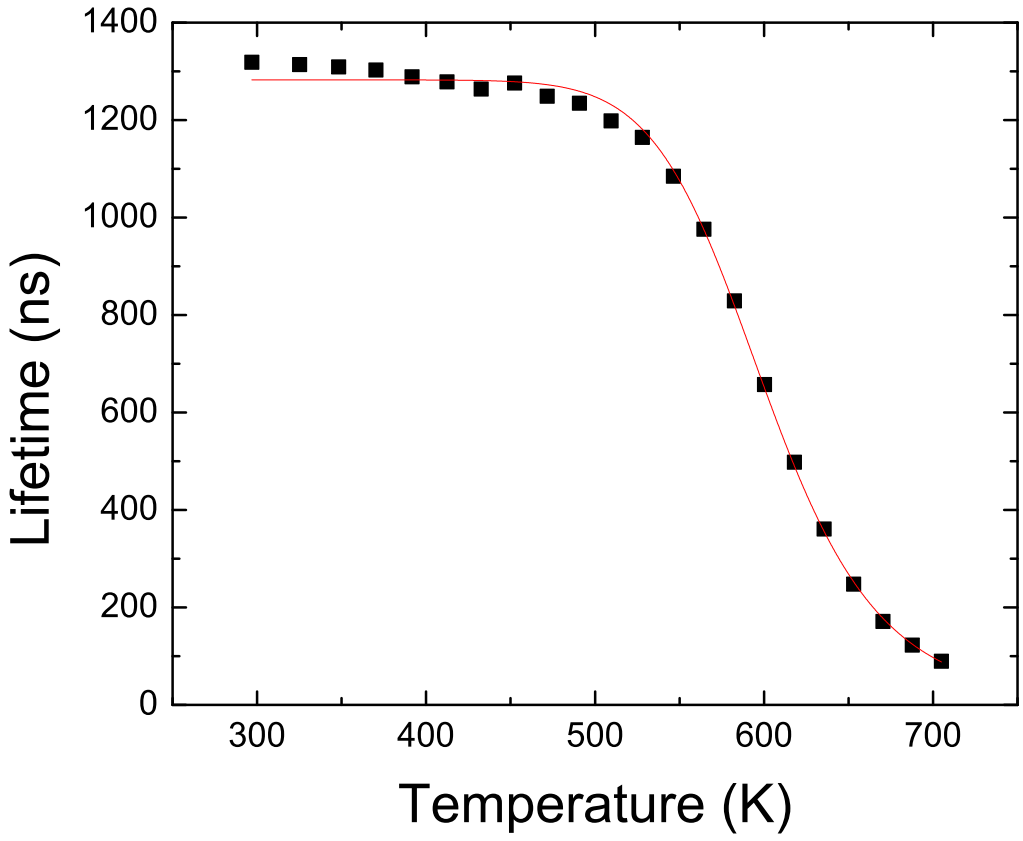

Figure 4.7: Arrhenius plot for $Cs_2CaP_2O_7$:Eu^{2+} which is a measure of emission lifetime versus temperature. The red curve is the Arrhenius model curve fit of Equation 4.8 to the data.

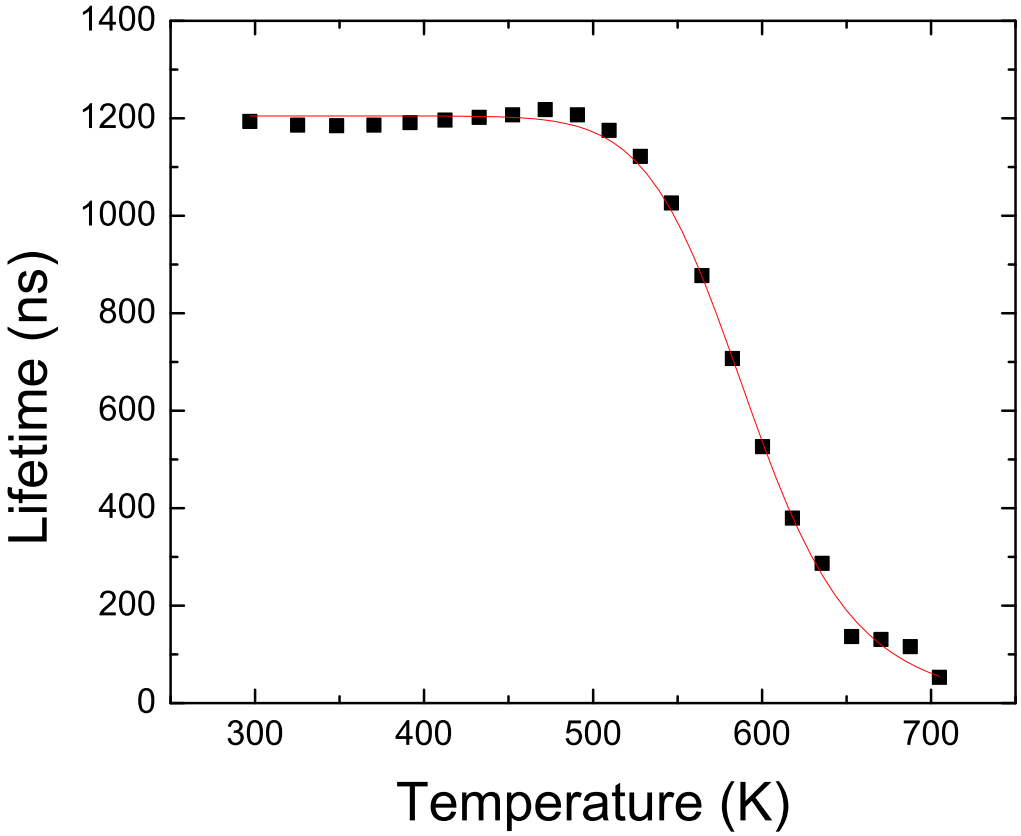

Figure 4.8: Arrhenius plot for $Cs_2SrP_2O_7$:Eu^{2+} which is a measure of emission lifetime versus temperature. The red curve is the Arrhenius model curve fit of Equation 4.8 to the data.

Phosphor	$\tau_o(\mu s)$	$\tau_{NR}(\mu s)$	$\Delta E(cm^{-1})$	$T_{0.5}$ (K)
$Cs_2CaP_2O_7$:Eu^{2+}	1.3	2.63×10^{-14}	7394	600
$Cs_2SrP_2O_7$:Eu^{2+}	1.2	7.14×10^{-15}	7900	600

Table 4.3: The Values of the Parameters used in fitting the temperature dependence of the lifetime data, the activation energy for thermal quenching (ΔE), and the thermal quenching temperature $T_{0.5}$.

been observed in other phosphates such as $Sr_3(PO_4)_2$ and $Ba_3(PO_4)_2$ where $T_{0.5} > 550$ K [52] and also in the oxynitride $SrSi_2O_2N_2$ where $T_{0.5}$ is close to 600 K [53].

4.6 The Centroid Shift and the Red Shift

The centroid shift (ϵ_c) is defined as the average of the Eu^{2+} $4f^6 5d^1$ electronic configuration relative to that of the free ion value. For Eu^{2+} in octahedral coordination, ϵ_c can be estimated as [54]

$$\epsilon_c = E_c^{free} - \left(E^{ex} + c + \frac{10Dq}{r} \right) \tag{4.10}$$

where E_c^{free} is the barycenter energy of the high spin $4f^6[^7\mathrm{F}]5d^1$ level in Eu^{2+} ion (4.93 eV) and for octahedral symmetry, $r = 5/2$ [54]. The factor $c = 0.37$ for Eu^{2+}. It is a correction factor that accounts for the difference between E^{ex} and the barycenter energy of the first Eu^{2+} ($4f^7[^8\mathrm{S}_{7/2}] \rightarrow 4f^6 5d^1[t_{2g}]$) excitation band in $Cs_2M^{2+}P_2O_7$(M = Ca, Sr):Eu^{2+} which is ~ 0.77 eV wide (see Table 4.2). It can therefore be calculated that for $Cs_2CaP_2O_7$:Eu^{2+} $\epsilon_c = 4517$ cm^{-1} (0.56 eV) and for $Cs_2SrP_2O_7$:Eu^{2+} $\epsilon_c = 4194$ cm^{-1} (0.52 eV).

The centroid shift in these materials is comparatively small. This indicates that the covalent bonding between the Eu^{2+} and the O^{2-} in $Cs_2M^{2+}P_2O_7$(M = Ca, Sr):Eu^{2+} is weak. This is not unusual because the Eu^{2+}–O^{2-} bonding is expected to be more ionic due to the strong covalency within the phosphate groups.

The shift in energy away from the free ion energy of a defect ion is known as the red shift, $D(2+, A)$ for divalent lanthanides in a given host material A. This value is indicative of both the strength of the crystal field splitting and the centroid shift. It can be determined from the following

$$D(2+, A) = E^{free} - E^{ex} \tag{4.11}$$

Where E^{free} is the energy difference between the ground state and the $4f^6[^7\mathrm{F}_0]5d^1$ excited state in the free ion level (34036 cm^{-1}, 4.22 eV in Eu^{2+}). One can see from Table 4.3 that the red shift for $Cs_2CaP_2O_7$:Eu^{2+} is larger than that of $Cs_2SrP_2O_7$:Eu^{2+} because of both the larger centroid shift and the larger crystal field splitting for the calcium sample.

4.7 References

[39] V.K. Trunov, Yu. V. Oboznenko, s.P. Sirotinkin and N.B. Tskhelashvili, Izvestiya Akademii Nauk SSSR, Neorganicheskie Materialy, **27**, 2370, (1991).

[40] I.V. Zatovsky, N, yu, Strutynska, N.S. Slobodyanik, V.N. Baumer, and O.V. Shishkin, Crystal Research and Technology, **43**, No.4, 362, (2008).

[41] N. Khay, A. Ennaciri, and A. Rulmont, Journal of Raman Spectroscopy, **32**, 1052, (2001).

[42] J. Hanuza, B. Jezowska, and K. Lukaszwicz, J. Mol. Struct. **13**, 391, (1972).

[43] B. C. Cornilsen, J. Mol. Stuct., **117**, 1, (1984).

[44] D. Philip, B. L. George, and G. Aruldhas, J. Raman Spectrosc., **21**, 523, (1990).

[45] N. C. Chang and J. B. Gruber, J. Chem. Phys., **10**, 3227, (1964).

[46] B. Henderson and G.F. Imbusch, *Optical Spectroscopy of Inorganic Solids*, Oxford University Press, Oxford, (1989).

[47] G. Blasse and A. Bril, Philips Res. Repts., **23**, 201, (1968).

[48] A.F. Wells, *Structural Inorganic Chemistry*, Clarendon Press, Oxford, (1950).

[49] P. Dorenbos, J. Lumin., **104**, 239, (2003).

[50] P. Dorenbos, J. Lumin., **91**, 155, (2000).

[51] P. Dorenbos, J. Phys.: Condens. Matter., **17**, 8103, (2005).

[52] S.H.M Poort, A. Meijerink and G. Blasse, J. Phys. Chem. Solids, **58**, 1451, (1997).

[53] V. Bachmann, T. Jüstel, A. Meijerink, C. Ronda, and P.J. Schmidt, J. Lumin., **121**, 441, (2006).

[54] P. Dorenbos, J. Phys.: Condens. Matter., **15**, 575, (2003).

[55] L. Pham, Ph.D. Dissertation, The University of Georgia, Athens, (2007).

[56] Z. Barandiaŕ,an, N.E. Edelstein, B. Ordejón, F. Ruiperez, and L. Seijo, J. Solid St. Chem., **178**, 464, (2005).

Chapter 5

Discussion

The excitation and emission characteristics of Eu^{2+} in $Cs_2CaP_2O_7$ and $Cs_2SrP_2O_7$ are very interesting. First, the emission bands are centered at 607 nm and 563 nm for the calcium and strontium samples respectively. These values are the farthest red-shifted emission peaks that have been reported in the literature concerning Eu^{2+} doped phosphate compounds. Second, the Stokes shift is very large ($\approx$ 1 eV) for both compounds. Third, the quenching temperature $T_{0.5}$ is high. Despite the large Stokes shift, the emission originates from a normal $4f^6 5d^1 \rightarrow 4f^7$ emission.

5.1 Eu^{2+} Excitation

For a free Eu^{2+} ion the $4f^6 5d^1$ absorption transition is observed at 33856 cm^{-1}. The free ion energies for Eu^{2+} and the other divalent lanthanides are schematically represented in figure 5.1. It is common to observe a staircase like structure in the excitation spectra. When the crystal field splitting is large, as found in many octahedrally coordinated compounds [57], the lowest step of the staircase is associated with the lowest $4f^6 5d^1$ level. Examples of well resolved spectra have been shown in $KMgF_3$ [58], EuF_2 [59], BaF_2 [60], and $Sr_3(PO_4)_2$ [61]. In such samples the energy level of the first $f \rightarrow d$ transition can be determined to within 500 cm^{-1}. Further, for octahedral crystal fields the Eu^{2+}excited $4f^6 5d$ levels are split into two bands. The lower energy band, t_{2g} is three fold degenerate and corresponds to the electronic wavefunctions occupying the positions off axis with respect to the ligands. The higher energy band e_g is two fold degenerate and those states arise from excitations along the ligand axes.

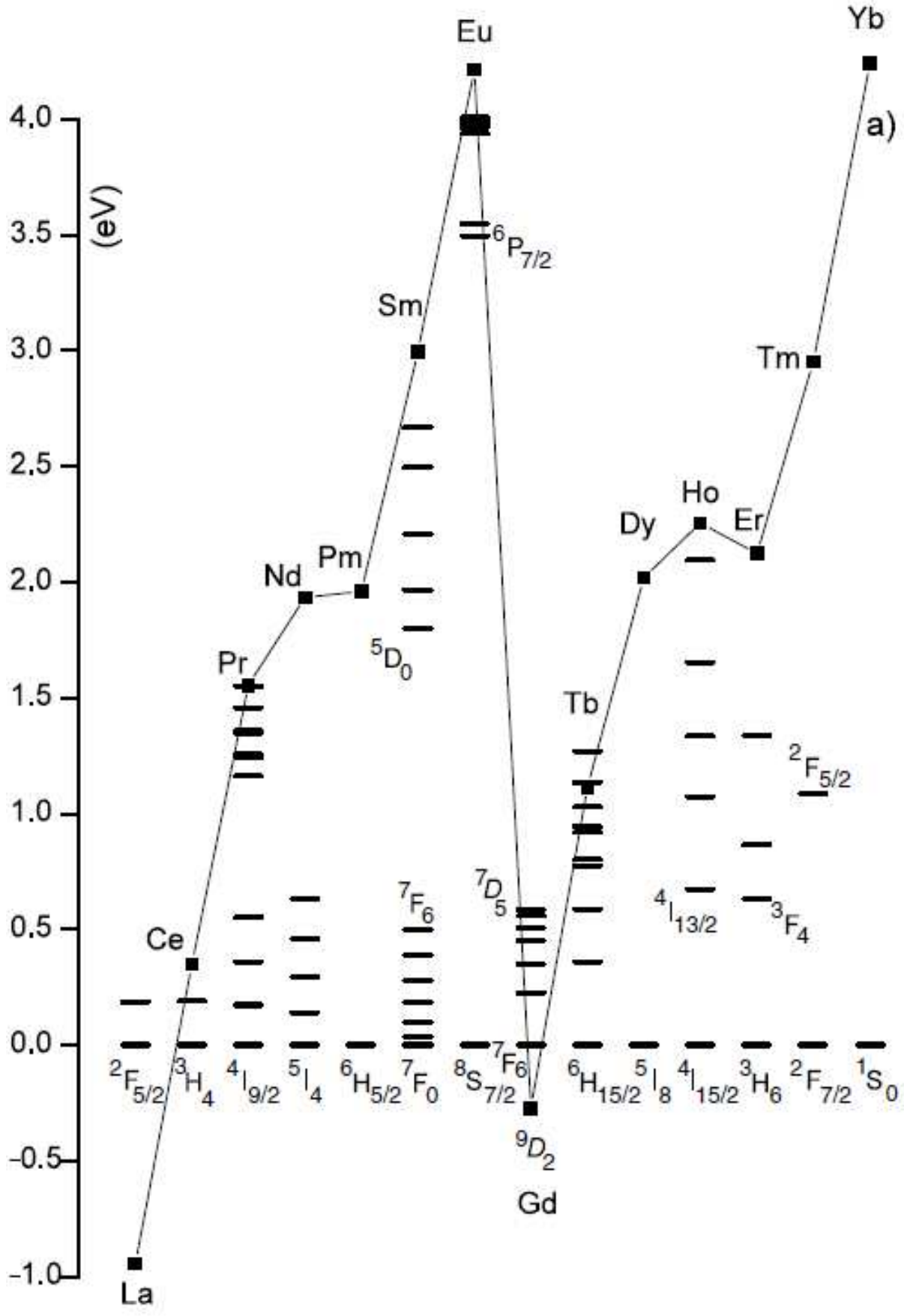

Figure 5.1: Free ion energies for the divalent lanthanides [73].

Some of the observed splitting in the excitation spectra of $Cs_2CaP_2O_7$ and $Cs_2SrP_2O_7$ may be due to a dynamic Jahn–Teller effect. According to the theory of Jahn and Teller, the symmetric nuclear configuration of an electronic state that is orbitally degenerate is unstable. For the case of octahedral symmetry, the three fold degenerate t_{2g} is unstable and through coupling to the lattice will be reconfigured in such a way as to remove the degeneracy. The phosphate groups to which the O^{2-} ligands are attached have large vibrational modes (1200 cm^{-1}) and provide a probable pathway for the distortion of the $4f^6 5d^1$ (t_{2g}) states. The extent of the distortion due to this effect is unclear because the theory makes no mention as to the magnitude of distortion that is necessary to remove degeneracy [62–64].

5.2 Eu^{2+} Emission Types

There are three basic types of emission associated with Eu^{2+} in inorganic solids [65]. Normal $d \rightarrow f$ broad band emission, $f \rightarrow f$ narrrow line emission, and "anomalous" emission. All three types involve excitation from the ground state to the $4f^6 5d^1$ levels of Eu^{2+} and the final state after emission is the $4f^7$ [$^8S_{7/2}$] ground state of Eu^{2+}.

5.2.1 Normal $d \rightarrow f$ Emission

Normal emission is characterized by the spin and dipole allowed *df* transitions. The electrons drop from the $4f^6 5d^1$ level back down to the $4f^7$ ground state. The band width of the transition is broad and usually lies between 1000 - 3000 cm^{-1}. The Stokes shift of such an emission is most frequently reported as < 4000 cm^{-1} [65]. Emission from this level is characterized by a high quenching temperature. The emission peak location does not shift upon changing temperature, and the radiative lifetime for such a transition is typically on the order of 700 μs.

5.2.2 Narrow line $f \rightarrow f$ Emission

This normal emission from the *df* levels in the divalent europium may sometimes be quenched by phonon relaxation from the excited 5d levels to that of the $4f^7$ configuration. Typically, this may occur when the $4f^7$ [$^6P_{7/2}$] level lies just below the lowest $4f^6 5d^1$ level. Upon excitation into the $5d$ state, a phonon relaxation allows the electron to cross into the $4f^7$ [$^6P_{7/2}$] which is followed by narrow line $^6P_{7/2} \rightarrow ^8S_{7/2}$ emission. This emission type is seen experimentally in both BaFCl:Eu^{2+} and SrFCl:Eu^{2+} [66]. Lifetimes for this type of emission are on the order of 100's of μs and is typically quenched at room temperature.

5.2.3 "Anomalous" Excitonic Emission

Anomalous emission is attributed to an impurity trapped exciton. Upon excitation of Eu^{2+} into the $4f^6 5d^1$ levels, the electron becomes ionized into the conduction band of the host material [67, 68]. The electron then becomes localized on the cations around the hole that was left on the Eu^{2+} impurity. Upon radiative transfer of this exciton back to the ground state of Eu^{2+} the "anomalous" emission occurs. Blasse, Lizzo et. al., and Poort et. al. have all reported cases of anomalous emission [69–71]. Dorenbos has detailed list of many other compounds that appear to demonstrate anomalous behavior [65]. Some characteristics associated with anomalous emission are:

1. The Stokes shift is very large (5000–10000 cm^{-1}).
2. The emission full width half maximum (Γ_{em}) is very broad (> 4000 cm^{-1}).
3. The lifetime of emission is generally longer than 100's of μs.
4. The emission intensity is usually quenched by 400 K.
5. The emission may show an anomalous temperature behavior. For example, the emission peak for $BaHfO_3$ shifts from 595 nm (4.2 K) to 479 nm (room temperature)[72].

This emission type is thought to involve conduction band states of the host compound and depend on the size of the lanthanide ion, the size of the site occupied, the size of the anions in the compound, and the binding strength of the oxygen ligands [73]. It has been reported that in certain compounds the $5d$ level of the impurity lanthanide can lie very close to the conduction band [67, 68, 70, 74–81] and this includes the Eu^{2+} ion. It is now generally accepted that the location of the $5d$ state relative to the conduction band states is directly related to the presence of anomalous emission. If the $5d$ level is close enough so that phonon absorption can autoionize the lanthanide or if the $5d$ level may actually lie within the conduction band, then anomalous emission is likely to occur. Another feature of anomalous emission is significant thermal quenching of the emission at temperatures below 400 K when the $5d$ level is close to the conduction band.

Figure 5.2 is a possible configuration coordinate diagram for an impurity lanthanide with several methods for relaxation from the d level excited state back to the ground state. To draw the diagram, realistic values from BaF_2:Eu^{2+} and SrF_2:Yb^{2+} data were used. Point A on parabola a represents the energy of the $4f^n$ ground state, where n is the number of f electrons. Next the electron is excited to the $5d$ level and point B on parabola b is reached. Due to lattice relaxation the system settles into point C on parabola b and from here several transition paths to the ground state may occur. In the case of SrF_2:Yb^{2+}, the system relaxes to the impurity-trapped exciton state indicated by point E on parabola d. The ray $\overrightarrow{EF}$ represents the anomalous emission. It can be characterized by a 0.6 eV wide (FWHM) and 1.55 eV high Stokes-shifted emission band. At room temperature, the BaF_2:Eu^{2+} system relaxes to point G on parabola e; this is followed by anomalous emission ($\overrightarrow{GF}$) at 590 nm. At low temperature, however, normal df emission at 403 nm ($\overrightarrow{CD}$) with a small Stokes shift of 0.17 eV has been reported for BaF_2:Eu^{2+}. Parabola c represents an excited state of the $4f^n$ configuration. Via the crossing point with parabola d, the anomalous emission is quenched and the excited $4f^n$ state becomes populated. The existence of the $^7F_6$ and $^2F_{5/2}$ levels in Sm^{2+} and Tm^{2+} is very likely the reason that anomalous emission has never been

observed for these lanthanides. It has only been observed for Eu^{2+} and Yb^{2+}, precisely those lanthanides where excited 4fn levels, that may quench anomalous emission, are absent.

Eu^{2+} is the most stable divalent lanthanide due to its half-filled ($4f^7$) valence shell. Dorenbos has compiled a list of the spectroscopic properties of Eu^{2+} in over 300 different compounds (fluorides, chlorides, bromides, iodides, oxides, sulfides, selenides, and nitrides). At 293 K the average values are $\Delta S \approx 1350$ cm^{-1} and $\Gamma_{em} \approx 1600$ cm^{-1}[65]. Although these are the expected values, there remains a very broad range in which one can expect to find the normal emission values.

5.3 Arguments Against Excitonic Emission

5.3.1 Stokes Shift

The stokes shifts in $Cs_2CaP_2O_7$ and $Cs_2SrP_2O_7$ are abnormally large in both materials. This observation is in accord with the assignment of anomalous emission to the emission peaks of the calcium and strontium samples. However, in general, a large Stokes shift may be indicative of substantial geometric distortions around the Eu^{2+} in the excited state. These distortions could also be due in part to noticeable movement of the Eu^{2+} ion from its central position and this could further be agitated by rotational distortions by the phosphate groups upon optical excitation. These types of distortions have been reported in Ce^{3+} doped halides and in $LaPO_4$. Moreover, with the $\langle Eu^{2+}–O^{2-}\rangle$ bond distances shortening in the excited state upon $4f^6 \rightarrow 5d(t_{2g})$ excitation, then this will lead to large crystal field splitting. All of this will lead to a shift to lower energy for the $4f^6 5d^1$ emission and result in a larger Stokes shift.

In fact, the large Stokes shift is not so much of an unusual characteristic for *df* emission transitions for octahedrally coordinated rare earth ions. For example, the Stokes shift of 6373 cm^{-1} (0.79 eV) and 8474 cm^{-1} (1.05 eV) have been reported for the Ce^{3+} *df* emission transition in the elpasolites, Rb_2NaScF_6 and Cs_2NaYF_6 respectively [83]. These values are

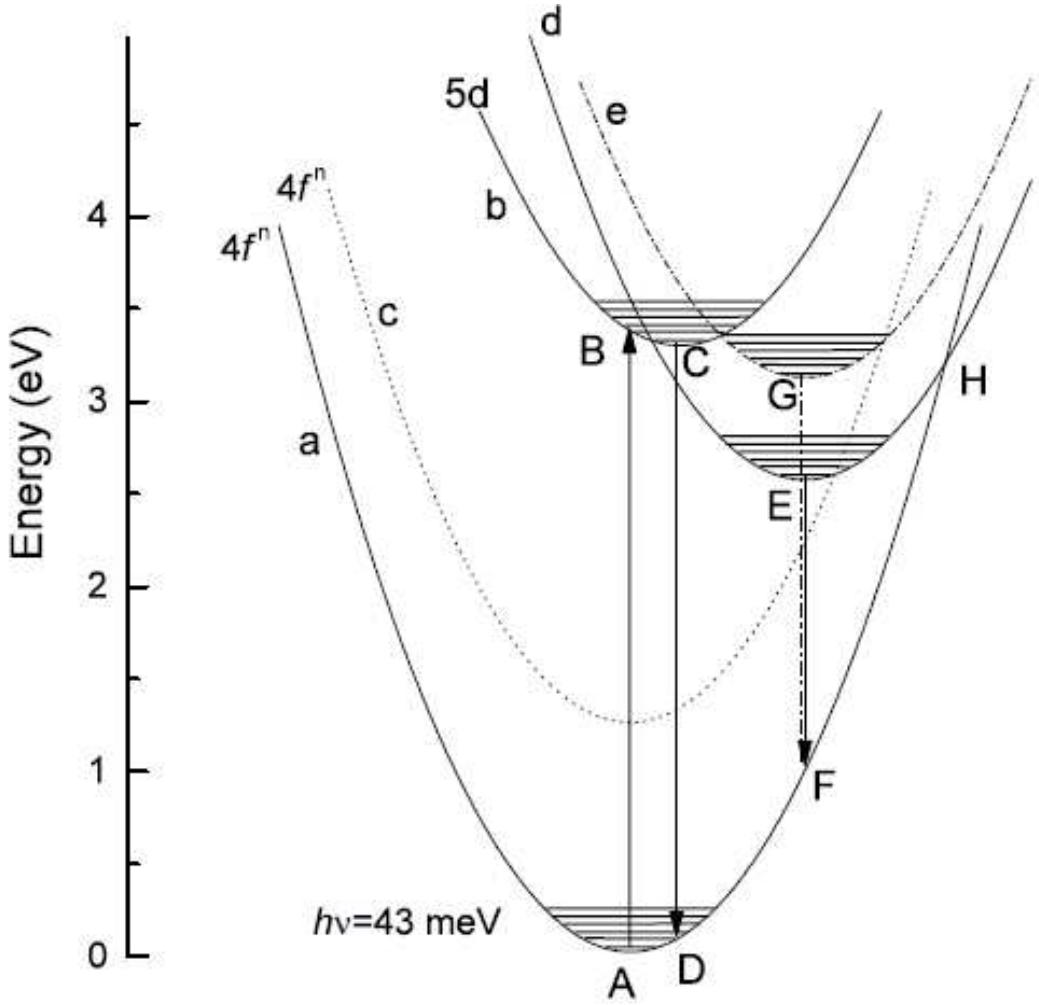

Figure 5.2: In this configurational coordinate diagram, there are several bands represented. Each parabola represents a different method of excitation/relaxation. There can be level crossing and this adds to the complexity of defining the results for real systems. [82].

very large compared to the average literature reported value of 2200 cm^{-1} (0.27 eV) [84] for Ce^{3+} emission in solids.

5.3.2 Emission Band Width

The full width half maximum for the emission band, Γ_{em} is very broad in divalent europium compounds exhibiting anomalous emission. Γ_{em} in the $Cs_2CaP_2O_7$ and $Cs_2SrP_2O_7$ samples are relatively narrow (2361 cm^{-1} and 2394 cm^{-1} respectively) compared with that of anomalous emission. Further, the width of emission here is described by the large coupling of the $4f^6 5d^1$ excited state to the lattice.

5.3.3 Lifetime

The characteristic lifetime of the normal Eu^{2+} $4f^6 5d^1 \rightarrow 4f^7[^8S_{7/2}]$ emission transition is around 1.2 μs. Data from Dorenbos regarding anomalous emission in compounds are compiled in Table 5.3.3 [65]. It is seen that, with the exception of Sr_2LiSiO_4F, the lifetimes representing an anomalous emission are all longer than 1.1 μs.

Specifically, the case of Eu^{2+} activated $Ba_2Mg(BO_3)_2$ ($\tau_{4.2K} = 12.6$ μs) is instructive since it exhibits an unusually long lifetime [86]. This longer lifetime is indicative of the anomalous emission due to the impurity trapped excitonic state of the Eu^{2+} ion. The values of the $Cs_2M^{2+}P_2O^7$:Eu^{2+} is $\sim 1.2\mu$s, and this is associated with the normal emission transition.

5.3.4 Thermal Quenching of the Eu^{2+} Emission

A low emission quenching temperature is one of the associated factors related with anomalous emission, however, it is most definitely not the sole indicator for an impurity trapped exciton level. Normal Eu^{2+} emission may quench at relatively low temperatures if the excited $4f^6[^7F_0]5d^1$ level is located close to the conduction band. This case has been encountered in Eu^{2+} activated $SrSiO_3$ and $CaSiO_3$ with $T_{0.5}$ near 100 K [86]. The Stokes shift of the emission is small (1500–1900 cm^{-1}) with $\tau_{4.2K}$ =0.7 μs. Since the lifetime is suggestive of the normal

emission, the impurity trapped exciton is not the lowest energy state in $SrSiO_3$ and $CaSiO_3$. The quenching temperature of the normal Eu^{2+} emission depends on the band gap of the host lattice.

The thermal quenching temperatures listed in Table 5.3.3 are all relatively low. $T_{0.5}$ ranges from 80 K for BaF_2 to 460 K for $BaSi_2O_5$. The quenching temperatures in $Cs_2M^{2+}P_2O^7$:Eu^{2+} are much higher ($T_{0.5} = 600$ K). Both the $T_{0.5}$ and the lifetime values indicate that the states of the Eu^{2+} $4f^6 5d^1$ electronic states are well isolated from the host lattice conduction band.

Comparing the values $T_{0.5}$ and E_{an}^{em} in Table 5.3.3 to the present materials under investigation is particularly interesting. It is seen that, with the exception of BaF_2, all of the materials exhibit an increase in $T_{0.5}$ with the increasing energy of the emitted photon E_{an}^{em}. This is contrary to the low emission energy and high $T_{0.5}$ of $Cs_2M^{2+}P_2O^7$:Eu^{2+}.

5.3.5 Emission Peak Stable with Temperature

For anomalous emission, there is a shift of the emission peak (on the order of 100's of nanometers) toward shorter wavelengths as the temperature increases e.g. BaF_2:Eu^{2+} [66, 68]. The emission spectra of Eu^{2+} in $Cs_2CaP_2O_7$ and $Cs_2SrP_2O_7$ do shift by 15 nm to shorter wavelength when the temperature is increased from $T = 77$ K to 573 K. However, this is a slight change relative to that of anomalous emission and is expected due to the decreasing crystal field strength at increasing temperatures.

5.4 Future Work

A natural progression of this work is to substitute for the alkali metal (Rb for Cs) and observe the changes in optical properties. Upon changing to $Rb_2CaP_2O_7$ and $Rb_2SrP_2O_7$, the lattice constant decreases and thereby increases the crystal field strength. The room temperature emission spectrum of $Rb_2SrP_2O_7$:Eu^{2+} has recently been measured. The emission peak maximum is located near 576 nm (17360 cm^{-1}). This is a shift to lower energy with respect to $Cs_2SrP_2O_7$:Eu^{2+} (17475 cm^{-1}) as is expected with an increased crystal field strength. This

result suggests that the observation of Eu^{2+} emission in $A_2MP_2O_7$ compounds (A = Cs, Rb; M = Ca, Sr) is from the normal $4^6 5d^1 \rightarrow 4f^7$ transition. However, a complete optical characterization of these compounds is necessary to validate this claim.

5.5 References

[57] P. Dorenbos, J. Lumin., **108**, 301, (2004).

[58] A. Ellens, A. Meijerink, and G. Blasse, J. Lumin., **59**, 293, (1994).

[59] M.J. Freiser, S. Methfessel, and F. Holtzberg, J. Appl. Phys., **39**, 900, (1968).

[60] R.L. Fuller and D. McClure, J. Lumin., **38**, 193, (1987).

[61] S.H.M. Poort, J.W.H. van Krevel, R. Stomphorst, A.P. Vink, and G. Blasse, J. Solid State Chem., **122**, 432, (1996).

[62] H.A. Jahn and E. Teller, Proc. Roy. Soc. (London), **A161**, 220, (1937).

[63] H. L. Schläfer and G. Gliemann, *Basic principles of ligand field theory*; translated from the German by D. F. Ilten., Wiley-Interscience, New York, (1969).

[64] C.K. Jørgensen, *Modern aspects of ligand field theory*,North-Holland Pub. Co., Amsterdam, (1971).

[65] P. Dorenbos, J. Lumin., **104**, 239, (2003).

[66] T. Kobayasi, S. Mroczkowski, and J.F. Owen, J. Lumin., **21**, 247, (1980).

[67] D.S. McClure and C. Pedrini, Phys. Rev. B, **32**, 8465, (1985).

[68] M. Moine, C. Pedrini, and B. Courtois, J. Lumin., **50**, 31, (1991).

[69] G. Blasse, Eur. J. Solid State Inorg. Chem., **33**, 175, (1996).

[70] S. Lizzo, E.P. Klein Nagelvoort , R. Erens, A. Meijerink, and G. Blasse, J. Phys. Chem. Solids, **58**, 963, (1997).

[71] S.H.M. Poort, H.M. Reijnhoud, H.O.T. van der Kuip, and G. Blasse, J. Alloys Compounds, **241**, 75, (1996).

[72] W.J. Schipper, D. van der Voort, P. van den Berg, Z.A.E.P. Vroon, and G. Blasse, Mat. Chem. Phys., **37**, 311, (1993).

[73] P. Dorenbos, J. Phys.: Condens. Matter., **15**, 575, (2003).

[74] B. Moine, B. Courtois, and C. Pedrini, J. Physique, **50**, 2105, (1989).

[75] S. Lizzo, A. Meijerink, and G. Blasse, J. Lumin., **59**, 185, (1994).

[76] S. Lizzo, A. Meijerink, G.J. Dirksen, and G. Blasse, J. Phys. Chem. Solids, **7**, 959, (1995).

[77] S. Lizzo, A. Meijerink, G.J. Dirksen, and G. Blasse, J. Lumin., **63**, 223, (1995).

[78] S.H.M. Poort, W.P. Blokpoel, and G. Blasse, Chem. Mater., **7**, 1547, (1995).

[79] S.H.M. Poort and G. Blasse, J. Lumin., **7274**, 247, (1997).

[80] R. Jagannathan and T.R.N. Kutty, J. Lumin., **71**, 115, (1997).

[81] Li-Ji Lyu and D.S. Hamilton, J. Lumin., **48/49**, 251, (1991).

[82] P. Dorenbos, J. Phys.: Condens. Matter., **15**, 2645, (2003).

[83] P. Dorenbos, J. Lumin., **91**, 155, (2000).

[84] P. Dorenbos, J. Andriessen, M. Marsman, and C.W.E. Van Eijk, Rad. Effects and Defects in Solids, **154**, 237, (2001).

[85] P.E. Smet, J.E. Van Haecke, F. Loncke, H. Vrielinck, F. Callens, and D. Poelman, Phys. Rev. B, **74**, 035207, (2006).

[86] S.H.M Poort, A. Meijerink and G. Blasse, J. Phys. Chem. Solids, **58**, 1451, (1997).

[87] M. Yamaga, Y. Masui, S. Sakuta, N. Kodama, and K. Kaminaga, Phys. Rev. B, **71**, 205102, (2005).

[88] W.J. Schipper, J.J. Piet, H.H. de Jager, G. Blasse, Mater. Res. Bull., **29**, 23, (1994).

Host	E^{ex}	E^{em}_{an}	ΔS	Γ^{em}_{an}	$T_{0.5}$ (K)	$\tau(\mu s)$ 4.2 K/RT	Ref
BaS	18315	11389	6925	3980	∼200	Afterglow	[85]
$Ba_2LiB_5O_{10}$	26697	15808	10807	2419 (4 K)	320	2.9/1.1	[65, 84, 86]
$Ba_2Mg(BO_3)_2$	24196	16453	7743	3791	340	12.6/5.4	[65, 84, 86]
Ba_3SiO_5	-	16949	-	2581	∼420	2.7 (100 K)	[87]
BaF_2	26132	17179	9195	4113 (77 K)	80	1.8/-	[65, 84, 86]
$Sr_3(BO_3)_2$	20620	17301	3306	4033 (4 K)	>150	2.5/-	[73, 88]
Sr_2LiSiO_4F	25000	18712	6210	3952	450	1.2/1.1	[65, 73, 86]
$BaSi_2O_5$	-	19196	-	-	460	3.3/3.1	[86]

Table 5.1: The optical properties of the Eu^{2+} ion in materials suspected of supporting anomalous emission; E^{em}_{an} is the peak energy of emission band; Γ^{em}_{an} is the full width at half maximum of the emission band; τ is the lifetime at 4.2 K and room temperature. All values are in cm^{-1} unless otherwise noted.

Chapter 6

Summary

The very large Stokes shift for these materials is in conflict with the general experience of the normal Eu^{2+} luminescence. Generally, a large Stokes shift is associated with anomalous emission related to self trapped excitons. However, based on the evidence of normal radiative lifetimes ($\sim$ 1.2 μs) and extremely high quenching temperatures of luminescence and the normal range of the full width half maximum values, it is concluded that the Eu^{2+} emission in $Cs_2M^{2+}P_2O_7$ originates from the lowest t_{2g} state of the $4f^6 5d^1$ electronic configuration and is a normal $d \rightarrow f$ emission.

The reasons for the observed luminescent characteristics arise from the substantial reduction of energy and increased splitting of the $^8S_{7/2}$ ground and $^5D_0$ first excited states for the $Cs_2M^{2+}P_2O_7$(M = Ca, Sr):Eu^{2+} crystals. Γ_{em} (the emission full width half maximum), τ_{em} (the radiative lifetime), and T_q (the thermal quenching temperature) are all well within normal limits and are consistent with normal *df* emission in Eu^{2+} containing compounds. This means that the $5d$ levels in Eu^{2+} do not cross over into the conduction band, and the the emission characteristics demonstrate the farthest $D(2+, A)$ (redshift) observed to date in phosphates.